Solute Probes of Conformational Changes in Open Complex (RP_o) Formation by *Escherichia coli* RNA Polymerase at the λP_R Promoter: Evidence for Unmasking of the Active Site in the Isomerization Step and for Large-Scale Coupled Folding in the Subsequent Conversion to RP_o†

Wayne S. Kontur,‡,|| Ruth M. Saecker,*,‡,|| Caroline A. Davis,§ Michael W. Capp,‡ and M. Thomas Record, Jr.*,‡,§

Departments of Chemistry and of Biochemistry, University of Wisconsin—Madison, Madison, Wisconsin 53706

Received September 9, 2005; Revised Manuscript Received November 23, 2005

ABSTRACT: Transcription initiation is a multistep process involving a series of requisite conformational changes in RNA polymerase (R) and promoter DNA (P) that create the open complex (RP_o). Here, we use the small solutes urea and glycine betaine (GB) to probe the extent and type of surface area changes in the formation of RP_o between Eσ^{70} RNA polymerase and λP_R promoter DNA. Effects of urea quantitatively reflect changes in amide surface and are particularly well-suited to detect coupled protein folding events. GB provides a qualitative probe for the exposure or burial of anionic surface. Kinetics of formation and dissociation of RP_o reveal strikingly large effects of the solutes on the final steps of RP_o formation: urea dramatically increases the dissociation rate constant k_d, whereas GB decreases the rate of dissociation. Formation of the first kinetically significant intermediate I_1 is disfavored in urea, and moderately favored by GB. GB slows the rate-determining step that converts I_1 to the second kinetically significant intermediate I_2; urea has no effect on this step. The most direct interpretation of these data is that recognition of promoter DNA in I_1 involves only limited conformational changes. Notably, the data support the following hypotheses: (1) the negatively charged N-terminal domain of σ^{70} remains bound in the "jaws" of polymerase in I_1; (2) the subsequent rate-determining isomerization step involves ejecting this domain from the jaws, thereby unmasking the active site; and (3) final conversion to RP_o involves coupled folding of the mobile downstream clamp of polymerase.

Kinetic studies of the process of open complex (RP_o)[1] formation by *Escherichia coli* RNA polymerase holoenzyme (R: catalytically competent core enzyme, $\alpha_2\beta\beta'\omega$ bound to promoter DNA-recognizing σ^{70} subunit, also abbreviated Eσ^{70}) at the λP_R promoter (P) have demonstrated that a minimum of three steps, involving two kinetically significant intermediates (I_1 and I_2), are required to describe the mechanism (*1*−*4*):

$$R + P \underset{k_{-1}}{\overset{k_1}{\rightleftarrows}} I_1 \underset{k_{-2}}{\overset{k_2}{\rightleftarrows}} I_2 \underset{k_{-3}}{\overset{k_3}{\rightleftarrows}} RP_o \qquad \text{(Mechanism I)}$$

rapid equilibrium; slow; slow; rapid equilibrium

Evidence for at least two kinetically significant intermediates has also been found for open complex formation at the *lac*UV5 (*5*), T7A1 (*6*−*9*), and λP_{RM} up 1 promoters (*10*). Although the structures of these intermediates (I_1, I_2) may be promoter-dependent (e.g., the extent to which DNA from −5 to +25 (where +1 is the start site) is protected by the "jaws" of RNAP in I_1, cf. refs *9*, *11*−*13*), all proposed mechanisms for RP_o formation at σ^{70} promoters invoke a critical slow (rate-determining) isomerization step after formation of a first kinetically significant intermediate, I_1. For λP_R, this slow step follows a sequence of rapidly equilibrating steps that form I_1 from free polymerase and promoter DNA. I_1 and all previous complexes are unstable to a 10 s challenge with competitor, whereas I_2 and RP_o (competitor-resistant (CR) complexes) survive this challenge.

For λP_R, the interconversion between intermediates I_1 and I_2 is the rate-limiting step in both the forward and back directions (*1*−*4*). In the forward direction, k_2 increases strongly with increasing temperature. The dependence of k_2 on temperature corresponds to a large, temperature-independent activation enthalpy (34 ± 2 kcal mol^{-1}) proposed to reflect protein rearrangements that nucleate DNA melting (*2*, *3*, *11*). In the back direction, k_{-2} is the slow step following

† This research was supported by NIH Grant No. GM23467 to M.T.R. W.S.K. was supported by NIH Biotechnology Training Grant No. 5 T32 GM08349.

* To whom correspondence should be addressed at 433 Babcock Drive, Madison, WI 53706. Phone, 608-262-5332; fax, 608-262-3453; e-mails, record@biochem.wisc.edu (for M.T.R.), rmsaecker@wisc.edu (for R.M.S.).

‡ Department of Chemistry, University of Wisconsin—Madison.

§ Department of Biochemistry, University of Wisconsin—Madison.

|| These authors contributed equally to this work.

[1] Abbreviations: ASA, water-accessible surface area; bp, base pair; DBD, DNA binding domain; Eσ^{70}, *E. coli* RNA polymerase holoenzyme; EM, electron microscopy; GB, glycine betaine; I_1, first kinetically significant intermediate; I_2, second kinetically significant intermediate; ·OH, hydroxyl radical; RNAP, RNA polymerase; RP_o, open complex; wt, wild-type.

10.1021/bi051835v CCC: $33.50
Published on Web 01/25/2006

the $RP_o \rightleftarrows I_2$ rapid equilibrium, yielding the composite dissociation rate constant $k_d = k_{-2}/(1 + K_3)$. The observed reduction in k_d with increasing temperature demonstrates the existence of the second intermediate I_2. Both the magnitude of activation enthalpy (~30 kcal mol^{-1} at ~15 °C) and the heat capacity change of dissociation indicate that large conformational changes also occur in the final steps, presumably including the propagation of DNA melting (*3*).

What is the correspondence between these data and movements in the polymerase machinery that occur in DNA opening? The combination of kinetic, biochemical, and genetic studies of $E\sigma^{70}$ and high-resolution structural descriptions of the homologous thermophilic enzymes (*14*, *15*) has led to distinct hypotheses for the sequence of conformational changes that form RP_o (including DNA bending, kinking, unwinding, and/or unstacking and protein folding, unfolding, and/or hinge bending) (*2*, *14*, *16*). To date, direct evidence exists for only one large-scale protein rearrangement in the process of bacterial RP_o formation: movement of the single-stranded DNA mimic region 1.1 of σ^{70} out of the DNA binding channel (*17*). Smaller-scale conformational changes are deduced from a comparison of crystal structures of the free *Thermus aquaticus* holoenzyme and that bound to a "forked" promoter DNA fragment (double-stranded from −41 to −12; single-stranded overhang of the nontemplate strand from −11 to −7). Upon binding, the β' "pincer" or "clamp" moves ~3 Å, and the position of the β-flap domain (bound to σ^{70} region 4) shifts ~6 Å (*15*, *18*). These relatively small shifts contrast with the large flexibility inherent in the multidomain structures of free σ^{70} and core. For example, conserved regions 2 and 4 of σ^{70} move some 15 Å apart upon binding core (*19*), and a comparison of EM and crystal structures suggests that the β/β' jaws of core polymerase can "flex" from ~25 to 50 Å apart (*20*). Is this flexibility exploited during open complex formation, and, if so, when?

Mapping structural transitions onto individual steps of RP_o formation is challenging due to the intrinsic instability of kinetic intermediates and the difficulty in obtaining a relatively homogeneous population of a given intermediate for study. In favorable cases, homogeneous populations of intermediates have been obtained by forming complexes at (or downshifting to) low temperature (cf. refs *5*, *11*, *21*−*23*). For example, early complexes (I_1 or earlier species, presumably on the pathway to forming RP_o) have been characterized at binding equilibrium at low temperature, which slows or prevents their conversion to later intermediates (cf. refs *11*, *13*, *21*, *24*, *25*), and at short times of reaction (*9*, *10*, *22*). Attempts to characterize I_2 at λP_R by $KMnO_4$ footprinting after temperature downshifts (*11*, *23*, *26*) appear to be complicated by the fact that the intrinsic $KMnO_4$ reactivity of the thymine bases in the open region of RP_o may be strongly temperature-dependent ((*27*); Capp, M. W., unpublished work). To date, neither the amount nor the positions of DNA opening in I_2 have been unambiguously determined by downshift experiments. Outside of demonstrations of its existence, I_2 (and other possible intermediates after it in rapid equilibrium on the time scale of $I_2 \rightarrow (I_1-I_2)^{\ddagger}$) remain virtually uncharacterized.

We have previously used temperature effects as a signature of conformational changes in the individual steps of open complex formation, finding that both the equilibrium constant (K_1) for formation of the first intermediate I_1 ($R + P \rightleftarrows I_1$) and the rate constant (k_d) for dissociation of RP_o ($RP_o \rightleftarrows I_2 \rightarrow I_1$) exhibit large temperature dependences characterized by large-magnitude heat capacity changes (ΔC_p^o) (*2*, *3*, *28*). A universal contribution to ΔC_p^o in protein processes arises from changes in the amounts of water-accessible nonpolar and polar surface area (ΔASA) (*29*−*32*). For protein folding, protein−protein interactions with coupled folding, and other processes where the surface buried is largely nonpolar, changes in ASA are quantitatively predicted by the observed negative ΔC_p^o (cf. ref *29*).

For formation of protein−nucleic acid interfaces, changes in polar and charged surface are typically as large or larger than changes in nonpolar ASA. As a result, the net contribution to ΔC_p^o from formation of the interface is predicted to be small in magnitude as a result of compensation between contributions from the burial of nonpolar and polar ASA. However, large negative ΔC_p^o characterize most protein−nucleic acid interactions studied to date. In some cases, protein folding coupled to binding contributes significantly to this effect, as originally proposed (*29*). In other cases, other coupled processes have been proposed, including DNA base unstacking (*33*, *34*), protonation (*35*), and disruption of protein surface salt bridges (*36*). Contributions of these latter processes to ΔC_p^o are not proportional to the corresponding changes in ASA. Since all of these coupled processes may be involved in the steps of RP_o formation, other probes of large-scale coupled folding and other coupled processes are needed.

In this study, we exploit the small biochemical solutes urea and glycine betaine (*N*,*N*,*N*-trimethyl glycine; GB) as probes of changes in polar amide (nitrogen, oxygen in amide groups) and anionic (carboxylate, phosphate) biopolymer surface, respectively. Combining quantitative data for the effects of urea on the unfolding of globular proteins (*32*) and α-helices (*37*) and for the interaction of urea with DNA and various native protein surfaces, we deduced that urea interacts principally with the polar amide surface of proteins and nucleic acid bases (*38*) and that, to a good approximation, the urea dependence of an equilibrium or rate constant of a process can be directly interpreted in terms of the change in polar amide surface area (ΔASA_{amide}; Å^2) involved (*39*)

$$\left(\frac{\partial \ln K_{obs}}{\partial m_{urea}}\right)_{a_{salt}}^{m_{urea}\rightarrow 0} = ((1.4 \pm 0.3) \times 10^{-3})\Delta ASA_{amide} \quad (1)$$

The use of urea as a quantitative probe of changes in exposure of polar amide surface in a protein−DNA interaction has been calibrated for the specific 1:1 binding of *lac* repressor (LacI) to SymL operator DNA (*39*). The amount of polar amide surface area buried in forming a 1:1 tetramer−operator complex, predicted from the initial slope of the urea dependence of the binding constant at constant salt activity ($\partial \ln K_{obs}/\partial m_{urea} = -2.1 \pm 0.2\ m^{-1}$) is 1500 ± 300 Å^2. This agrees quantitatively with the amount of polar amide surface predicted to be buried from structural data (*40*, *41*), 1526 Å^2 (of which 491 Å^2 is buried in the LacI−DNA binding interface, 515 Å^2 in coupled folding of the hinge helices, and 520 Å^2 in the protein−protein interface formed by docking of the folded DBD on the core domain of repressor (*39*)). Notably, two-thirds of the magnitude of the initial slope arises from the burial of amide ASA in coupled conforma-

tional changes, even though these changes only contribute one-half of the *total* amount of surface buried. Thus, we conclude that urea is particularly suitable for detecting protein folding events and creation of protein−protein interfaces in protein−nucleic acid interactions (*39*).

The use of GB as a quantitative probe of anionic surface was also tested in the study of LacI binding to SymL (*39*). GB increases the LacI−SymL binding constant as expected for a complex that buries 632 Å^2 of DNA phosphate surface. However, the initial slope of the binding constant at constant salt activity ($\partial \ln K_{obs}/\partial m_{GB} = 1.8 \pm 0.2$ m^{-1}) predicts that 450 ± 100 Å^2 of anionic surface is buried. We (*39*) proposed a possible explanation for this quantitative discrepancy: a weak favorable preferential interaction of GB with multiple exposed aromatic residues on the DBD of LacI (Tyr 7 and Tyr 17), by analogy with the aromatic binding site observed in the crystal structure of GB bound to the ProX porter (*42*). If the cation−π interactions seen in the GB−ProX crystal structure are generalizable, GB would oppose formation of any interface that buries previously exposed aromatic residues, while favoring burial of DNA phosphates. Such an interaction with the native state of the LacI DBD would explain its unexpectedly large stabilization by GB (*43*) as well as the unexpectedly small stabilization of the LacI−SymL complex by GB. In addition, effects of GB on processes that wrap DNA nonspecifically on a protein surface (e.g., integration host factor, nucleosome assemblies) may be complicated (see Discussion). Although interactions of GB with different types of biopolymer surfaces appear to be substantially more complicated than effects of urea, systems investigated to date exhibit a strong correlation between large effects of GB and large-scale burial or exposure of anionic surface (*38*, *39*, *43*).

Here, we determine the effects of urea and GB on the rate and equilibrium constants of steps or portions of the RNAP−promoter association mechanism (I), and use these to discuss extant proposals for the mechanism of open complex formation. This approach has the distinct advantage of probing structural changes as they occur on the pathway. A rate constant can be analyzed using eq 1 in the same manner as that used for an equilibrium constant. According to transition state theory, the rate constant for a process (k) is proportional to the equilibrium constant for conversion of the reactant(s) of that process to the subsequent transition state ($K_{obs}^{\ddagger}$). Assuming that the transition state decomposition frequencies in the coefficient of proportionality are independent of urea concentration, the urea dependence of the logarithm of the rate constant is equal to the urea dependence of the log of the equilibrium constant for the formation of the transition state: $\partial \ln k/\partial m_{urea} = \partial \ln K_{obs}^{\ddagger}/\partial m_{urea}$. Thus, $\partial \ln k/\partial m_{urea}$ is proportional to the amount of polar amide surface area exposed or buried in the formation of the transition state.

EXPERIMENTAL PROCEDURES

Buffers. Different buffers and reaction conditions were employed in different series of experiments to optimize the quality and range of data that could be collected for each. This optimization was based on preliminary data collected under various reaction conditions.

For the study of the effect of urea concentration on the kinetics of irreversible association of RNAP and λP_R promoter DNA, binding buffer (BB_{urea}^{assoc}) contained 0.086 molal (m) KCl, 0.036 m Tris-HCl (pH 8.0 at 25 °C), 0.014 m NaCl, 0.0032 m $MgCl_2$, 0.947 m glycerol, 0.001 m DTT, 100 μg/mL BSA, and 0, 0.33, 0.66, or 1.01 m urea. For the study of the effect of GB concentration on the kinetics of association of RNAP and λP_R promoter DNA, binding buffer (BB_{GB}^{assoc}) contained 0.107 m KCl, 0.044 m Tris-HCl (pH 8.0 at 28 °C), 0.014 m NaCl, 0.0086 m $MgCl_2$, 0.948 m glycerol, 0.001 m DTT, 100 μg/mL BSA, and 0, 0.69, or 1.47 m GB. Effects of urea on the kinetics of dissociation of competitor-resistant (CR) complexes were investigated at 17.1 °C in BB_{urea}^{dissoc} (0.123 m KCl, 0.010 m $MgCl_2$, 0.041 m Tris-HCl (pH 8.0 at 17.1 °C), 0.003 m NaCl, 0.001 m DTT, 100 μg/mL BSA, 0.20 M glycerol, and 0−0.63 m urea). Effects of GB on the kinetics of dissociation were investigated at 17.1 °C in BB_{GB}^{dissoc} (0.126 m KCl, 0.010 m $MgCl_2$, 0.041 m Tris-HCl (pH 8.0 at 17.1 °C), 0.003 m NaCl, 0.001 m DTT, 100 μg/mL BSA, 0.52 m glycerol, and 0−0.65 m GB).

To keep the concentrations of all solution components whose effects are not being studied constant on the molal scale, the stock solutions of both urea and GB were made by dissolving solid urea or GB monohydrate into previously prepared BB. As GB was used in its monohydrate form, the additional water introduced with the GB reduced the molalities of the other components in BB_{GB}^{assoc} and BB_{GB}^{dissoc} slightly. At the highest GB concentration studied (1.47 m), these reductions were <1.5% for all solution components; the effects of these changes in molal concentration were calculated to be negligible. In the case of BB_{urea}^{dissoc}, for convenience, solid urea was dissolved into solvent containing final concentrations of every component except for glycerol, so that a constant molarity of glycerol was obtained in these experiments (increasing the molality of glycerol slightly (insignificantly) from 0.24 to 0.25 m with increasing urea concentration).

Storage Buffer (SB) for RNAP holoenzyme, core deletion mutants (ΔSI1 and ΔSI3), and σ^{70} subunit consists of 6.8 M glycerol (50% v/v), 10 mM Tris-HCl (pH 7.5 at 4 °C), 100 mM NaCl, 0.1 mM dithiothreitol (DTT), and 0.1 mM Na_2-EDTA.Wash Buffer (WB) for nitrocellulose filter binding assays consists of 0.1 M NaCl, 10 mM Tris-HCl (pH 8.0 at room temperature), and 0.1 mM Na_2EDTA.

Wild-Type Eσ^{70} RNA Polymerase Holoenzyme. E. coli K12 wild-type RNA polymerase holoenzyme was purified and stored in individual 500 μL samples as described (*2*). Promoter binding activities of RNAP samples were determined at the time of use by analysis of forward titrations of promoter DNA with RNAP performed in BB in the complete binding of limiting reagent regime at 37 °C as described (*1*) and used to calculate the concentrations of active holoenzyme reported here. Wild-type Eσ^{70} RNAP preparations used in this study were 40−60% active. No systematic differences in promoter association kinetics were found between RNAP preparations when corrected for activity.

Core Deletion Mutants, ΔSI1, and ΔSI3. Mutant RNAP core enzymes (ΔSI1, deletion of residues 226−350 of β, and ΔSI3, deletion of residues 943−1130 of β') were generous gifts of I. Artsimovitch in the form of BL21 *E. coli* cells containing plasmids pIA329 and pIA331 (*44*). The published method of preparation (*44*) was used to purify both ΔSI1 and ΔSI3, with slight modifications. During this procedure,

RNA contamination was detected in the sample using an agarose gel stained with Gelstar (Cambrex, Rockland, ME). Therefore, 0.22 mg/mL RNase was pumped through the chitin column after the sample had been loaded. While this eliminated the RNA, a small amount of RNase was present in the final sample.

Alternatively, ΔSI3 was prepared by overexpressing α, *β*, and *β′*ΔSI3 (containing a hexa-histidine tag at the C-terminus) from plasmid pIA321 (which carries an ampicillin-resistant marker, also a gift from I. Artsimovich) using the autoinduction method of ref *45* and purification protocol described in ref *44*. *β′*ΔSI3 was extensively dialyzed against SB and stored at −70 °C. Working stocks were thawed and stored at −20 °C and reconstituted with σ^{70} as described below. No difference in dissociation kinetics was observed between chitin-tagged and his-tagged RNAP.

Wild-Type E. coli σ^{70}. Wild-type *E. coli* σ^{70} was purified as described (*46*), with the following modifications. Larger buffer volumes were generally used to resuspend cell and protein pellets. The resuspended protein pellet was diluted 2-fold with reconstitution buffer, instead of denaturing buffer. It was dialyzed against buffer E, instead of reconstitution buffer. The sample was first run through a Q-Sepharose anion-exchange column, then a 6 mL S-Sepharose cation-exchange column, instead of just a DEAE-Toyopearl TSK 650M column. The protein was found to be >90% pure σ^{70}.

λP_R Promoter DNA. A ^{32}P-DNA fragment containing the λP_R promoter was 3′-end-labeled and purified as described in ref *47*. *BssH* II and *Sma* I cleavage of pBR81 centrally positions the λP_R wild-type sequence (−60 to +20) in a fragment which extends from −115 to +76 relative to the transcription start site (+1) of the promoter. The specific activity of the fragment was generally ∼10^8 cpm/mol.

Dissociation Kinetics. Effects of urea and GB on the kinetics of dissociation of preformed CR complexes were determined for wild-type RNAP, ΔSI1, and ΔSI3 in 0−0.63 *m* urea, and for wild-type RNAP in 0−0.65 *m* GB. Dissociation was made irreversible by the addition of an excess of heparin, and the kinetics of decay were monitored at 17.1 °C in the appropriate BB^{dissoc} using nitrocellulose filter binding. Polyanionic heparin is found to be an inert (i.e., nondisplacing) competitor, both in the presence and absence of urea and GB; rates of dissociation at 0 and 0.63 *m* urea are independent of heparin concentration in the range 50−400 μg/mL (data not shown). Heparin was also shown to be an effective competitor for free RNAP in experiments in which free RNAP, initially incubated with heparin at 100 μg/mL, subsequently did not bind promoter DNA (data not shown). For experiments with ΔSI1 and ΔSI3, holoenzyme was reconstituted by incubating wild-type σ^{70} subunit with mutant core in at least a 1.5:1 molar ratio in SB on ice for at least 45 min before commencement of the experiment.

λP_R DNA (0.08−0.09 nM) and RNAP (10−40 nM for wild-type, 5 or 5.8 nM for ΔSI1, 1.7 or 16 nM for ΔSI3) were combined in the appropriate BB^{dissoc} (± urea or GB) and incubated for at least 1 h at 17.1 °C in a water bath to allow association to proceed to equilibrium. At time $t = 0$, 50 μL of heparin in the appropriate BB^{dissoc} (at 17.1 °C; final concentration: 100 μg/mL) was combined with the 1450 μL reaction. At recorded time points, 100 μL aliquots were removed and filtered at room temperature. Two independent experiments were performed for each unique combination of holoenzyme construct (wild-type, ΔSI1, or ΔSI3) and urea or GB concentration studied. Before heparin was added, 100 μL was removed from the reaction and transferred to 37 °C, where it was incubated for at least 30 min, then combined with 3.45 μL of heparin (at 37 °C; final concentration: 100 μg/mL). After ∼10 s, 100 μL of this sample was filtered to determine the total amount of DNA capable of binding to RNAP, cpm_{37}.

Association Kinetics. The irreversible kinetics of formation of CR complexes stable to a brief (∼10 s) challenge by heparin (100 μg/mL final concentration) were measured as a function of urea (in BB^{assoc}_{urea} at 25 °C) or GB (in BB^{assoc}_{GB} at 28 °C) concentration using rapid quench mixing and nitrocellulose filter binding as detailed previously (*48*). In most cases, the DNA and RNAP solutions contained the same concentrations of the appropriate BB^{assoc} before being mixed. In some cases where the final desired concentration of RNAP was high, the RNAP sample contained a concentration of SB that was higher than that present in the final BB. Because the RNAP was stored in SB, increasing the concentration of RNAP required adding higher amounts of SB to the RNAP sample. In such cases, the DNA sample contained a concentration of SB that was correspondingly lower than that in the final BB, so that, after mixing the RNAP and DNA, the solution contained the final BB concentrations of all components. As a control, both procedures (using either matched or unmatched buffers) were compared at lower [RNAP]; no difference was seen between the two methods.

Final concentrations of λP_R DNA were 0.08−0.24 nM and of RNAP were 1.2−75.2 nM. All experiments contained at least a 5.4-fold excess of RNAP over λP_R DNA to ensure that the kinetics were pseudo-first order. At time *t*, the reaction was quenched and expelled from the loop into a total volume of ∼270 mL (including reaction sample, heparin, and push buffer), resulting in a final concentration of ∼86−100 μg/mL heparin. No effect of heparin concentration was seen over this range.

Nitrocellulose Filter Binding Assays. Nitrocellulose filter binding assays were performed as described (*2*). For dissociation reactions, the total counts per minute filtered (cpm_{TOT}, generally ∼1000−3500 cpm) was determined by spotting 20 μL of the reaction mixture onto a dried nitrocellulose filter. For association reactions, cpm_{TOT} was determined by performing a reaction with BB in the RNAP sample port and applying the entire sample onto three dried nitrocellulose filters. Filter efficiency (∼0.70−0.99) was determined by dividing cpm_{37} (for dissociation reactions) or the plateau $cpm_{t\to\infty}$ (for rapid mix association reactions) by cpm_{TOT} in a reaction. Cerenkov radiation (cpm) from dried filters was measured in a Hewlett-Packard Tri-Carb 2100 TR scintillation counter.

Data Analysis. All data were analyzed using SigmaPlot 6.0 (SPSS, Inc., Chicago, IL) on a Dell Optiplex GX270 running Windows XP Professional v. 2002.

Determination of Dissociation Rate Constants (k_d). Where kinetics of dissociation of CR complexes were single-exponential (in the absence of solute and in the presence of urea; see Results), observed rate constants k_d ($= k_{-2}/(1 + K_3)$, with $K_3 = k_3/k_{-3}$ (*2*, *49*)) were determined by fitting data for θ_t^{CR} (where $\theta_t^{CR} = cpm_t/(cpm_{37} - cpm_{bkgd})$ and

$cpm_t = cpm_{obs} - cpm_{bkgd}$) to

$$\theta_t^{CR} = \theta_0^{CR} e^{-k_d t} \quad (2)$$

where θ_0^{CR} is the value of θ_t^{CR} at time $t = 0$ (i.e., the initial fraction of DNA in CR complexes). For dissociation experiments in GB where the decay is not well-described by eq 2, the kinetics were empirically characterized by the half-time $t_{1/2}$ for complete dissociation. This was determined for each GB concentration (except for the 0 *m* control, which was well-fit by a single exponential) by smoothing the data in the midrange of θ_t^{CR} ($0.7 > \theta_t^{CR}/\theta_0^{CR} > 0.3$) by fitting it to a quadratic equation and determining the time at which $\theta_t^{CR} = 0.5\theta_0^{CR}$, using the initial time point (taken within 25 s of mixing with heparin) as θ_0^{CR}.

Determination of Composite Forward Rate Constants (α_{CR}). In general, for each combination of RNAP and urea or GB concentration studied, association reactions were performed in duplicate (the only exception being the reactions at 0.66 *m* urea, each of which was only performed once). For each set of duplicates, the forward rate constant (α_{CR}) was determined by fitting the data ($\theta_t^{CR} = cpm_t/cpm_{t\to\infty}$) to a single-exponential rise to a plateau:

$$\theta_t^{CR} = 1 - e^{-\alpha_{CR} t} \quad (3)$$

For a preliminary set of data performed under the conditions used for the dissociation reactions, the association reaction was reversible (wherein an equilibrium distribution of free RNAP and DNA, I_1, and CR complexes is reached); these data required a relaxation analysis involving subtraction of k_d from relaxation rate constant β_{CR} to calculate α_{CR} (see Supporting Information).

Determination of K_1 and k_2 from the RNAP Concentration Dependence of α_{CR}. For single-exponential kinetics in excess RNAP ($[RNAP]_T \gg [promoter\ DNA]_T$, where $[RNAP]_T$ represents the total active concentration of RNAP in a reaction), α_{CR} is a hyperbolic function of RNAP concentration (*2*)

$$\alpha_{CR} = \frac{K_1 k_2 [RNAP]_T}{1 + K_1 [RNAP]_T} = \frac{k_a k_2 [RNAP]_T}{k_2 + k_a [RNAP]_T} \quad (4)$$

where $k_a \equiv K_1 k_2$ is the composite overall second-order association rate constant, K_1 ($= k_1/k_{-1}$) is the equilibrium constant for formation of the first kinetically significant intermediate (I_1, in rapid equilibrium with free RNAP and DNA), and k_2 is the microscopic rate constant for the subsequent (rate-determining; $k_2 < k_{-1}$) conversion of I_1 to I_2. (For convenience, the subscript T is dropped from $[RNAP]_T$ below.) Values of α_{CR} (weighted by $1/\sigma^2$, where σ is the standard deviation) were plotted versus [RNAP] and fit to eq 4 to determine K_1 and k_2 at any given set of conditions.

Urea and GB Concentration Dependences of Equilibrium and Kinetic Constants. Plots of $\ln K_1$ versus solute (GB, urea) molality exhibit curvature; solute dependences of $\ln K_1$ were therefore fit as a quadratic function of molality. The logarithms of other kinetic constants (k_2, k_d, $t_{1/2}$) were well-fit by a linear dependence on solute molality. Fits were weighted by $1/\sigma^2$, where σ is the standard deviation of $\ln X$.

Correction of Observed Solute Dependences for the Interactions of Solute with KCl and $MgCl_2$. Both urea and GB have slightly favorable interactions with KCl and $MgCl_2$ in solution (*50* and Capp, M. W., unpublished work). Therefore, addition of either solute will reduce the thermodynamic activities of KCl and $MgCl_2$ and thereby favors steps in open complex formation that are driven by a reduction in salt activity. Since our kinetics experiments were performed at constant molal concentrations of KCl and $MgCl_2$, and not at constant activities, a correction for the effects of urea and GB concentrations to constant KCl and $MgCl_2$ activities is necessary. In the Appendix, experimental osmotic and isopiestic data for the effects of urea and GB on the nonideality of KCl and $MgCl_2$ solutions are used to obtain these corrections, which are significant because of the strong effect of changes in salt activity on protein−nucleic acid interactions.

PONDR Predictions and ASA Calculations. The default predictor VL-XT of PONDR (Predictors of Natural Disordered Regions) was used to predict the degree of disorder in *Thermus thermophilus, T. aquaticus*, and *E. coli* β and β' subunits from their amino acid sequences (*51*, *52*). Sequences were submitted using the web interface at www.pondr.com. Surface areas were calculated as previously described (*30*).

RESULTS

Irreversible Dissociation Kinetics: Large Effects of Urea and GB on the Second Half of the Mechanism of Open Complex Formation. The effects of urea and GB on the kinetics of dissociation of competitor-resistant (CR) complexes (I_2, RP_o) provide information about the net burial or exposure of polar amide and anionic surfaces in the second half of the mechanism of open complex formation (after formation of the $(I_1-I_2)^{\ddagger}$ transition state between I_1 and I_2 in Mechanism I). Since the half-life of CR complexes at λP_R at moderate salt concentrations at $T \geq 25$ °C is inconveniently large (≥8 h), studies were performed at 17.1 °C, where k_d is more accurately determined. Kinetic data for irreversible dissociation of CR complexes in the presence of the competitor heparin were collected for a range of concentrations of urea (up to 0.63 *m*) and GB (up to 0.65 *m*) under otherwise identical reaction conditions. These data are plotted in Figure 1 as the fraction of promoter DNA in CR complexes, θ_t^{CR}, versus time. Urea and GB have large effects in opposite directions on the rate of dissociation of CR complexes; urea increases it, and GB decreases it.

For all urea concentrations investigated, Figure 1A demonstrates that dissociation of CR complexes fits well to a single-exponential time course (eq 2), decaying to zero at long times. Values of k_d (Table 1) increase strongly with urea concentration: k_d is approximately 7-fold faster in 0.63 *m* urea than in the absence of urea. At the urea concentrations in Figure 1A, k_d is smaller at 28 °C than at 17.1 °C (data not shown). These results indicate that the negative activation energy of dissociation characteristic of CR complexes in the absence of this solute persists in urea. We conclude from these data that the mechanism of dissociation of CR complexes in urea is described by a rapid equilibrium between RP_o and I_2 on the time scale of I_2 converting back to $(I_1-I_2)^{\ddagger}$ (*49*).

As shown in Figure 1B, addition of GB slows the entire time course of dissociation of CR complexes greatly. In

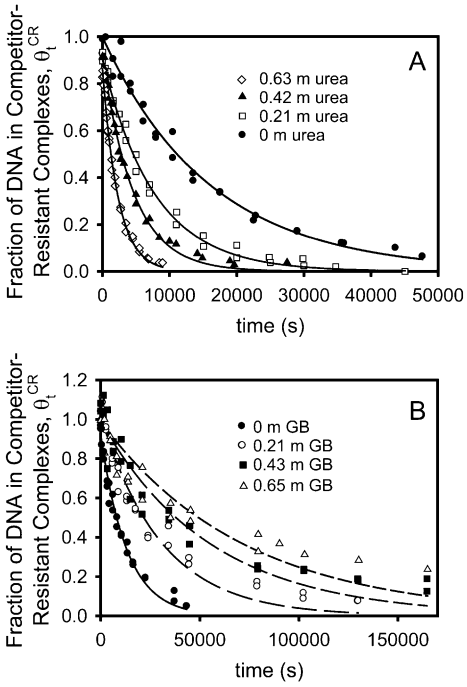

FIGURE 1: Effects of urea and glycine betaine (GB) concentration on the dissociation of competitor-resistant (CR) RNAP−λP_R complexes (I_2, RP_o). Decay of CR complexes at 17.1 °C in (A) BB_{urea}^{dissoc} (at 0, 0.21, 0.42, and 0.63 *m* urea) or (B) BB_{GB}^{dissoc} (at 0, 0.21, 0.43, and 0.65 *m* GB) is shown. Data are plotted as the fraction of promoter DNA bound to RNAP in CR complexes (θ_t^{CR}) versus time after addition of heparin to a final concentration of 100 μg/mL. Curves represent fits of the data to single-exponential decays, assuming complete dissociation of CR complexes (eq 2).

addition, in the range 0.21−0.65 *m* GB, only the first 60−70% of the dissociation reaction fits the exponential form of eq 2; the final 30−40% of the decay is slower than expected. Given the complexity of the decay of CR complexes in GB, we describe the effect of GB on dissociation in terms of an empirical half-time $t_{1/2}$ (see Experimental Procedures). Effects of GB on dissociation are large: the half-time $t_{1/2}$ is approximately 6-fold larger in 0.65 *m* GB than in the absence of GB. Evidence for conversion of open complexes formed at high temperature between T4 gp55 containing RNA polymerase and the T4 late promoter to a thermostable state at lower temperature has been obtained by $KMnO_4$ footprinting (*53*). To test if a corresponding process is induced by addition of GB, $KMnO_4$ footprints of CR complexes in the presence and absence of 0.6 M GB were compared (Davis, C. A., manuscript in preparation); no significant differences in either relative or absolute reactivities of thymines in the open region are detected.

The large effect of urea on k_d is symptomatic of large-scale coupled unfolding in the kinetically significant steps of dissociation, equivalent to large-scale coupled folding in the second half of the mechanism of open complex formation, as discussed below. To test whether either of two large insertions in the β (SI1, residues 226−350) or β' (SI3, residues 943−1130) subunits of *E. coli* RNAP contribute to the effect of urea on k_d, we characterized the effects of urea on the kinetics of dissociation on RNAP mutants lacking these insertions. As observed for wild-type polymerase, the kinetics of decay of CR complexes in urea are single exponential (Figure 2A,B); dissociation rate constants are listed in Table 1. The initial fraction of DNA in CR complexes in these experiments, θ_0^{CR}, is a function of both [RNAP] and urea concentration. For ΔSI1, θ_0^{CR} (determined from a combination of the two data sets at 5 and 5.8 nM RNAP in Figure 2A) decreases from ∼1 at 0 *m* urea to 0.3 at 0.63 *m* urea. For ΔSI3, θ_0^{CR} (from the representative data set at 16 nM RNAP in Figure 2B) decreases from ∼1 at 0 *m* urea to 0.8 at 0.63 *m* urea.

As observed previously on the T7 A1 promoter (*44*), both deletion mutants dissociate faster than wild-type polymerase from the λP_R promoter in the absence of urea (k_d increases 1.5-fold for ΔSI1 and 3-fold for ΔSI3 at 0 *m* urea under these solution conditions). However, Figure 2C (a semilogarithmic plot of k_d versus urea concentration for wild-type and the two mutants) reveals that this effect is not a function of urea concentration. A comparison of the slopes in Figure 2C shows that the urea dependences of k_d for wild-type RNAP, ΔSI1, and ΔSI3 are the same within error (Table 1).

Irreversible Association Kinetics as a Function of RNA Polymerase and Solute (Urea or Glycine Betaine) Concentrations. Initial experiments performed under the same solution conditions used to investigate dissociation indicated that effects of urea on K_1 and k_2 were relatively small in comparison to effects of urea on k_d. Under these conditions, association is reversible at low RNAP concentrations and/or higher urea concentrations. Therefore, a relaxation analysis is required to analyze the data (in which k_d is subtracted from the relaxation rate constant β_{CR} to get the composite association rate constant α_{CR}). Since this analysis increases the uncertainty, we were unable to quantify these relatively small effects of urea with sufficient accuracy (see Supporting Information). To quantify these effects, we found conditions where formation of CR complexes is irreversible, even in the presence of 1.01 *m* urea, and where K_1 is large enough so that k_2 can be accurately determined. These requirements were met by raising the temperature to 25 °C and by reducing

Table 1: Urea Concentration Dependence of the Dissociation Rate Constant k_d[a]

	k_d (s^{-1})		
m_{urea}	wild-type	ΔSI1	ΔSI3
0 *m*	$(6.2 \pm 0.3) \times 10^{-5}$	$(9.5 \pm 0.4) \times 10^{-5}$	$(1.9 \pm 0.1) \times 10^{-4}$
0.21 *m*	$(1.29 \pm 0.04) \times 10^{-4}$	$(1.76 \pm 0.06) \times 10^{-4}$	$(3.4 \pm 0.1) \times 10^{-4}$
0.42 *m*	$(2.17 \pm 0.06) \times 10^{-4}$	$(3.4 \pm 0.1) \times 10^{-4}$	$(6.4 \pm 0.3) \times 10^{-4}$
0.63 *m*	$(4.3 \pm 0.1) \times 10^{-4}$	$(5.1 \pm 0.3) \times 10^{-4}$	$(1.00 \pm 0.06) \times 10^{-3}$
$(\partial \ln k_d/\partial m_{urea})_{m_4,m_5}$	$3.0 \pm 0.1\ m^{-1}$	$2.7 \pm 0.2\ m^{-1}$	$2.7 \pm 0.1\ m^{-1}$
$(\partial \ln k_d/\partial m_{urea})_{a_4,a_5}$[b]	$3.2 \pm 0.1\ m^{-1}$	2.9 ± 0.2[c] m^{-1}	2.9 ± 0.1[c] m^{-1}

[a] Determined at 17.1 °C in BB_{urea}^{dissoc} (see Experimental Procedures). [b] Determined from eq A6 (see Appendix). [c] Determined assuming that the values of Sk_d for ΔSI1 and ΔSI3 are the same as those of wild-type RNAP.

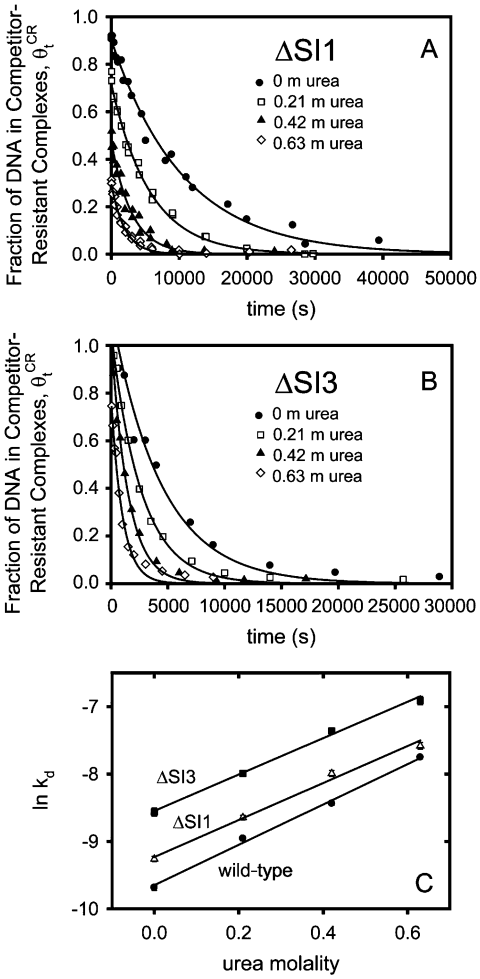

FIGURE 2: Effects of urea concentration on the dissociation of competitor-resistant (CR) complexes formed with the RNAP deletion mutants ΔSI1 and ΔSI3. Nitrocellulose filter binding data for the irreversible dissociation of CR complexes formed between (A) ΔSI1 RNAP (residues 226−350 deleted from the β subunit of RNAP) or (B) ΔSI3 RNAP (residues 943−1130 deleted from the β' subunit) and λP_R promoter DNA at 17.1 °C in BB_{urea}^{dissoc} are shown for various urea concentrations (0, 0.21, 0.42, and 0.63 *m*). Data are plotted as the fraction of DNA bound to RNAP in CR complexes (θ_t^{CR}) versus time. (Because the two data sets for ΔSI3 were taken at two significantly different RNAP concentrations, panel B shows a representative data set at 16 nM RNAP.) Curves represent fits of the data to single-exponential decays (eq 2); values of the rate constant k_d obtained from these fits are listed in Table 1. (For ΔSI3, values in Table 1 are averages of k_d from fits to individual data sets.) (C) Comparison of the effect of urea on the rate of dissociation of ΔSI1 (open triangles), ΔSI3 (filled squares), and wild-type (filled circles) RNAP−λP_R complexes. Solid lines are weighted linear fits of the data. Slopes of these fits are listed in Table 1.

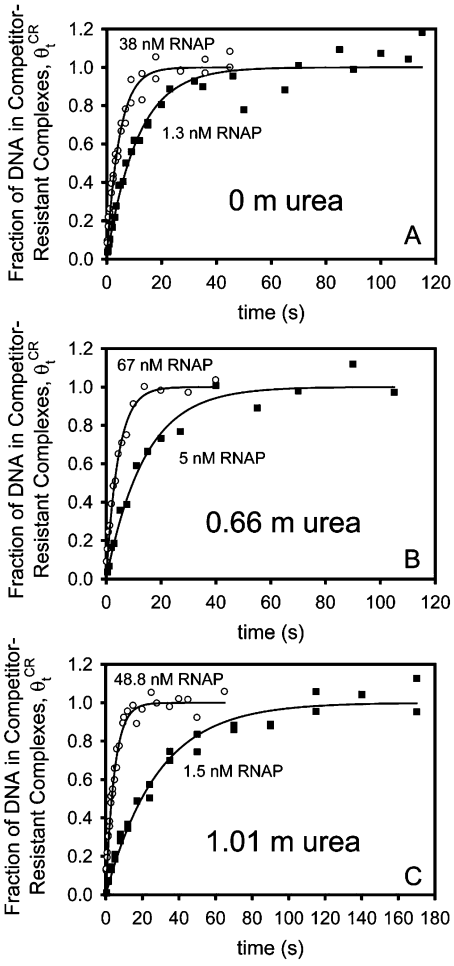

FIGURE 3: Effects of urea on the irreversible kinetics of formation of competitor-resistant (CR) complexes between RNAP holoenzyme and λP_R promoter DNA. Examples of rapid quench flow association kinetic data are shown for the highest and lowest RNAP concentrations studied at 0 (A), 0.66 (B), and 1.01 *m* (C) urea at 25 °C in BB_{urea}^{assoc}. Data are plotted as the fraction of promoter DNA in the form of CR complexes, θ_t^{CR}, as a function of time. Solid lines are fits of the data to irreversible single-exponential kinetics (eq 4, with $\theta_{eq}^{CR} = 1$).

the concentrations of KCl and $MgCl_2$ to those of BB_{urea}^{assoc}. The effects of GB on the association kinetics were also investigated under irreversible conditions (in BB_{GB}^{assoc} at 28 °C). At these temperatures, the kinetics are sufficiently fast that manual mixing cannot accurately determine k_2, necessitating the use of a rapid-quench mixer (*2*).

Representative data obtained at low (1.1−5 nM) and high (37−72.5 nM) RNAP concentrations at three concentrations of urea (0, 0.66, and 1.01 *m*) and GB (0, 0.69, and 1.47 *m*) are shown in Figures 3 and 4. In all cases, the association kinetics are single-exponential. Exponential fits of the kinetic data (to eq 4) are shown as the solid curves in Figures 3 and 4; these yield composite association rate constants α_{CR} for each RNAP and solute concentration investigated. Since the association mechanism is multistep, the observation of single-exponential kinetics indicates that the steps of initial binding and bending of promoter DNA to form the competitor-sensitive intermediate I_1 rapidly equilibrate on the time scale of the subsequent slow conversion of I_1 to I_2 (*2*, *49*).

To visualize the effects of urea concentration on the binding constant K_1 for formation of the intermediate I_1 and on the isomerization rate constant k_2, values of the association rate constant α_{CR} for each RNAP and urea concentration investigated are plotted in Figure 5. The behavior of α_{CR} as a function of RNAP concentration is clearly hyperbolic at each urea concentration, consistent with eq 4. A well-defined plateau value of α_{CR} in the accessible range of RNAP concentration is observed at each urea concentration. These plateau values of α_{CR} (attained at [RNAP] ≥ 30 nM; Figure 5A) are the same at all urea concentrations, revealing that the isomerization rate constant k_2 for $I_1 \rightarrow I_2$ does not depend significantly on urea concentration.

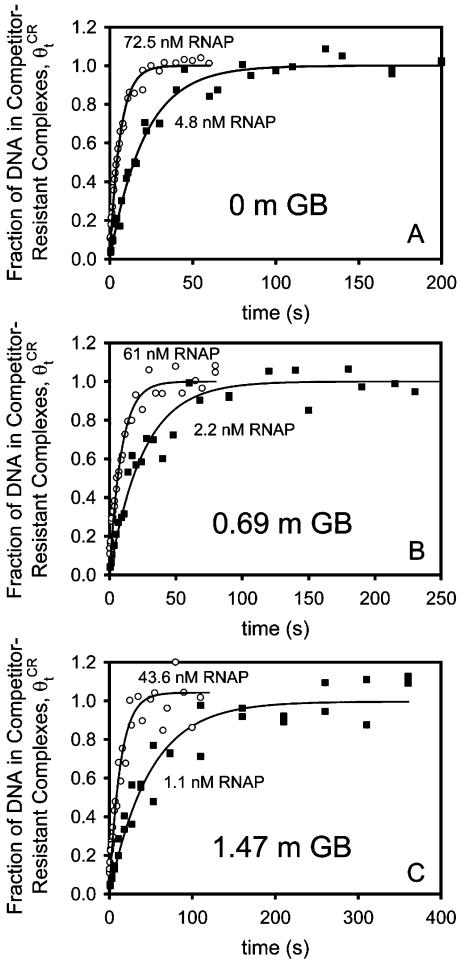

FIGURE 4: Effects of glycine betaine (GB) on the irreversible kinetics of formation of competitor-resistant (CR) complexes between RNAP holoenzyme and λP_R promoter DNA. Examples of rapid quench flow association kinetic data are shown for the highest and lowest RNAP concentrations studied at 0 (A), 0.69 (B), and 1.47 *m* (C) GB at 28 °C in BB_{GB}^{assoc}. Data are plotted as the fraction of promoter DNA in the form of CR complexes, θ_t^{CR}, as a function of time. Solid lines are fits of the data to irreversible single-exponential kinetics (eq 4, with $\theta_{eq}^{CR} = 1$).

At low RNAP concentration, the modest but significant reduction in α_{CR} at the higher urea concentrations investigated (observed more clearly in the expanded-scale Figure 5B) indicates that the equilibrium constant K_1 decreases at higher urea concentration. Significantly, the behavior of α_{CR} as a function of RNAP concentration at 0.33 *m* urea is the same within the uncertainty as in the absence of urea (Figure 5B); the effect of urea on α_{CR} at any low RNAP concentration clearly increases with increasing urea concentration. Fits of all α_{CR} to the hyperbolic eq 4 for the $R + P \rightleftarrows I_1 \rightarrow$ products mechanism are shown in both panels of Figure 5. These fits yield the values of K_1 and k_2 listed in Table 2.

Values of the association rate constant α_{CR} for each RNAP and GB concentration investigated are plotted in Figure 6. As observed with urea, α_{CR} is a hyperbolic function of RNAP concentration at each GB concentration; however, for GB, the well-defined plateau value of α_{CR} at high RNAP concentration decreases strongly with increasing GB concentration, revealing that k_2 decreases strongly with increasing GB concentration. At low RNAP concentration, on the other hand, α_{CR} is essentially independent of GB concentration, indicating that the equilibrium constant K_1 for formation of the intermediate I_1 must increase sufficiently with increasing GB concentration to compensate for the effect of GB on k_2, so that the low RNAP concentration limit of α_{CR} ($\alpha_{CR} \rightarrow K_1 k_2 [RNAP]_T$) is independent of GB concentration. Fits of the RNAP concentration dependences of α_{CR} to hyperbolic eq 4 at each GB concentration are shown in Figure 6, and values of the fitted quantities K_1 and k_2 are listed in Table 2.

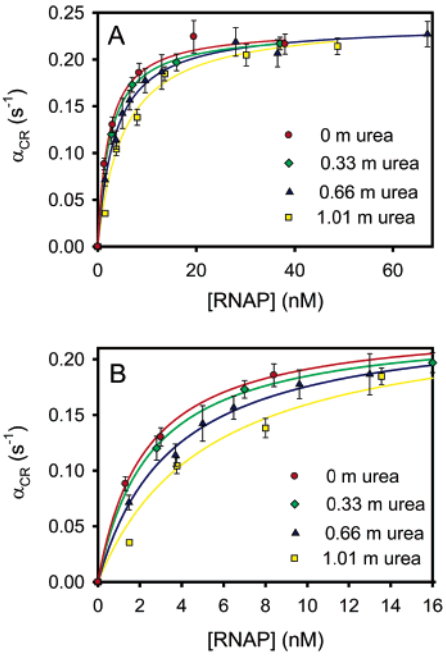

FIGURE 5: Effects of RNAP and urea concentrations on the composite association rate constant α_{CR}. (A) Values of α_{CR} obtained from all irreversible association kinetic experiments (see Figure 4 for examples) are plotted as a function of RNAP concentration at 0, 0.33, 0.66, and 1.01 *m* urea. The RNAP concentration scale of panel A emphasizes the lack of effect of urea on α_{CR} at high RNAP concentrations. Solid lines are fits of the data to eq 4; values of K_1 and k_2 determined from these fits are listed in Table 2. The expanded concentration scale plot in panel B shows the significant effect of urea on α_{CR} at low RNAP concentrations.

Table 2: Urea and GB Concentration Dependences of the Equilibrium Constant for Formation of I_1 (K_1) and the Forward Rate Constant for Conversion of I_1 to I_2 (k_2) in Mechanism I

25 °C (BB_{urea}^{assoc})		
	K_1 (M^{-1})	k_2 (s^{-1})
0 *m* urea	$(4.5 \pm 0.4) \times 10^8$	$(2.34 \pm 0.06) \times 10^{-1}$
0.33 *m* urea	$(4.0 \pm 0.3) \times 10^8$	$(2.31 \pm 0.03) \times 10^{-1}$
0.66 *m* urea	$(2.8 \pm 0.2) \times 10^8$	$(2.38 \pm 0.05) \times 10^{-1}$
1.01 *m* urea	$(1.9 \pm 0.3) \times 10^8$	$(2.43 \pm 0.12) \times 10^{-1}$
$(\partial \ln(K \text{ or } k)/\partial m_{urea})_{m_4,m_5}$	$-0.3 \pm 0.3\ m^{-1}$	$0.03 \pm 0.03\ m^{-1}$
$(\partial \ln(K \text{ or } k)/\partial m_{urea})_{a_4,a_5}$[a]	$-0.7 \pm 0.3\ m^{-1}$	$0.03 \pm 0.03\ m^{-1}$
28 °C (BB_{GB}^{assoc})		
	K_1 (M^{-1})	k_2 (s^{-1})
0 *m* GB	$(6.5 \pm 0.8) \times 10^7$	$(2.0 \pm 0.1) \times 10^{-1}$
0.69 *m* GB	$(1.5 \pm 0.4) \times 10^8$	$(1.4 \pm 0.1) \times 10^{-1}$
1.47 *m* GB	$(2.9 \pm 0.5) \times 10^8$	$(8.5 \pm 0.6) \times 10^{-2}$
$(\partial \ln(K \text{ or } k)/\partial m_{GB})_{m_4,m_5}$	$1.4 \pm 0.4\ m^{-1}$	$-0.6 \pm 0.1\ m^{-1}$
$(\partial \ln(K \text{ or } k)/\partial m_{GB})_{a_4,a_5}$[a]	$0.7 \pm 0.4\ m^{-1}$	$-0.6 \pm 0.1\ m^{-1}$

[a] Determined from eq A6 (see Appendix).

Analysis of Effects of Urea and GB on the Rate and Equilibrium Constants for the Steps of Open Complex

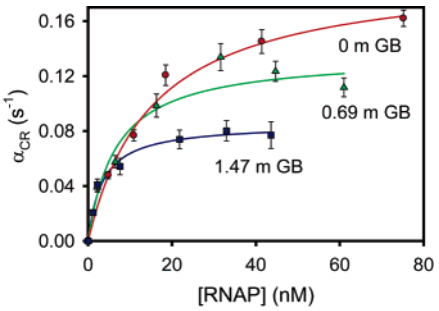

FIGURE 6: Effects of RNAP and glycine betaine (GB) concentrations on the composite association rate constant α_{CR}. Values of α_{CR} obtained from all irreversible association kinetic experiments (see Figure 5 for examples) are plotted as a function of RNAP concentration at 0, 0.69, and 1.47 *m* GB. Solid lines are fits of the data to eq 4; values of K_1 and k_2 determined from these fits are listed in Table 2.

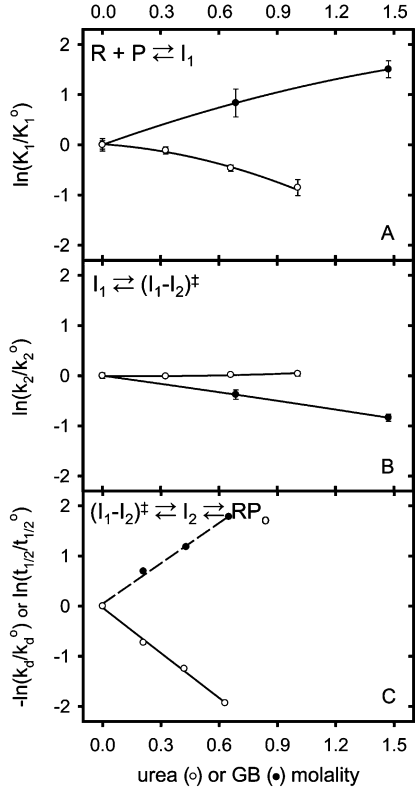

FIGURE 7: Summary of effects of urea and GB on the steps of the mechanism. Natural logarithms of K_1 (A), k_2 (B), and $1/k_d$ or $t_{1/2}$ (C) (all normalized to the appropriate values in the absence of solute) are plotted versus urea or GB concentration. (A) Solid lines represent quadratic fits to the data. (B and C) Solid lines represent linear fits of the $\ln k_2$ and $\ln k_d$ data, respectively; dashed line in panel C is for $\ln t_{1/2}$. Values of the slopes (for panel A, the initial slope) of the fits are listed in Tables 1 and 2, along with the corresponding quantities after correction to constant salt activity.

Formation. Figure 7 summarizes the results of irreversible association and dissociation kinetic studies (Figures 1, 5, and 6). Figure 7A plots the logarithm of the normalized equilibrium constant K_1 for formation of I_1 as a function of solute molality. Curvature is detected in the urea concentration dependence, as is observed for binding of LacI to SymL operator DNA in the range 0−3 *m* urea (*39*). This curvature may reflect a destabilization of some aspect of the free RNAP structure or of the polymerase assembly at the higher urea concentrations used here (possibly destabilization of the σ−core binding interaction). For this reason, the initial slope of the fit was used in subsequent calculations. The initial slope of the urea concentration dependence is negative, as expected for burial of polar amide surface in binding, but is small in magnitude ($(\partial \ln K_1/\partial m_{urea})^o = -0.3 \pm 0.3\ m^{-1}$); correction to constant salt (KCl and $MgCl_2$) activity does not increase the magnitude beyond that expected for the burial of polar amide surface of RNAP in the interface with promoter DNA (see Discussion) and provides no evidence for any large-scale coupled folding. The initial GB slope is positive ($1.4 \pm 0.4\ m^{-1}$), the direction expected for burial of anionic phosphate surface of DNA in forming I_1 (see Discussion).

For the subsequent, rate-determining conformational change, effects of urea and GB on the logarithm of the normalized rate constant k_2 are shown in Figure 7B. Remarkably, this step is essentially independent of urea concentration ($\partial \ln k_2/\partial m_{urea} = 0.03 \pm 0.03\ m^{-1}$; values of k_2 at all urea concentrations are the same within error), indicating that there is no detectable net change in exposure of amide surface in converting I_1 to the subsequent transition state $(I_1-I_2)^‡$. GB significantly reduces the rate of this step; the GB derivative of the logarithm of k_2 is $-0.6 \pm 0.1\ m^{-1}$, consistent with significant exposure of anionic surface in this step. The correction of the data to constant salt activity does not change this result detectably because the salt dependence of this step is small in magnitude ($Sk_2 \approx -1$; Kontur, W. S., manuscript in preparation). No curvature is detected in plots of $\ln k_2$ versus m_{solute} over the ranges examined.

Figure 7C plots the logarithm of the normalized inverse dissociation rate constant (for urea) or half-time (for GB) as a function of solute molality. Analyzed in this manner, the urea data are interpretable as effects on the conversion of the $(I_1-I_2)^‡$ transition state to the equilibrium mixture of RP_o and I_2 (presumably mostly RP_o) for the conditions investigated. Clearly, the effect of urea on these steps is dramatically greater than its effect on the steps of the first half of the mechanism ($-\partial \ln k_d/\partial m_{urea} = 3.0 \pm 0.1\ m^{-1}$); most of the polar amide surface buried in forming the open complex is buried in the second half of the association mechanism in conformational changes that occur after initial binding and formation of I_1. This situation is analogous to that observed for the effect of urea on the LacI−SymL interaction, where the majority (65−70%) of the urea effect results from conformational changes and only 30−35% is due to formation of the protein−DNA interface. Proposals for the late conformational changes in open complex formation detected by urea are given below. For GB, the situation is complicated by the fact that the final stages of the dissociation kinetics (Figure 1B) are not well-fit by a single-exponential decay. Even with this complication, it is clear that the latter half of the mechanism is more sensitive to GB concentration than either the initial binding step or the subsequent isomerization step.

For the overall process of CR complex formation from free RNAP and promoter DNA, the equilibrium constant K_{obs}^{CR} is the ratio of the composite forward rate constant k_a ($= K_1k_2$) to the dissociation constant k_d ($K_{obs}^{CR} = k_a/k_d$). Thus, the effect of urea on the overall process can be found from the individual effects on the forward and reverse processes: $(\partial \ln K_{obs}^{CR}/\partial m_3)_{a4,a5} = (\partial \ln K_1/\partial m_3)_{a4,a5} + (\partial \ln k_2/\partial m_3)_{a4,a5} -$

$(\partial \ln k_d/\partial m_3)_{a4,a5}$. The urea dependence of the overall process of CR complex formation at constant salt activity is -3.9 ± 0.3 m^{-1} (corresponding to a net burial of $(2.8 \pm 0.6) \times 10^3$ Å^2 of polar amide surface).

DISCUSSION

Open complex formation by Eσ^{70} RNAP involves a sequence of conformational changes in both polymerase and promoter DNA that create the transcription bubble and position the template strand in the active site. Here, we have exploited low (nondenaturing) concentrations of urea to probe protein conformational changes along the pathway. Similarly, we have used low concentrations of GB to detect changes in the water accessibility of anionic oxygens on the DNA backbone and polymerase (Asp, Glu side chains, C-termini). Strikingly we find the largest effects of both solutes on the final steps in the mechanism, indicating that large-scale motions in the polymerase machinery occur *after* the formation of an extensive interface with duplex promoter DNA (~−82 to +25; Davis, C. A., manuscript in preparation), as part of the descent from the high free-energy $(I_1-I_2)^{\ddagger}$ transition state to the final open complex.

We have recently proposed that the effects of urea concentration on an equilibrium or rate constant can be directly interpreted in terms of the amount of amide surface area exposed or buried in a process using the relationship ΔASA_{amide} (Å^2) = $(710 \pm 150)(\partial \ln \kappa/\partial m_{urea})$ where the derivative is taken at constant salt activity and at $m_{urea} \rightarrow 0$, and where κ is either an equilibrium or rate constant (eq 1; (*39*)). The dependence of $\ln(1/k_d)$ on m_{urea} reported here predicts that ~2300 ± 500 Å^2 of ASA_{amide} are buried in events that convert the $(I_1-I_2)^{\ddagger}$ complex to RP_o (see Table 1). This value of ΔASA_{amide} is 1.3 times greater than that found for the interaction between LacI and its high affinity symmetric operator site SymL (*39*), and similar to that buried when a small protein such as CheY or apomyoglobin forms its highly ordered native state from an extended, denatured state (see ref *39* and references therein). Notably, for LacI binding, two-thirds of the total of amide surface buried occurs outside of the LacI−SymL interface in protein interfaces created by folding of the hinge helices and docking of the DNA binding domain on the core domain of repressor. By analogy with repressor binding and protein folding data, the urea dependence of k_d provides strong evidence that a region or regions on polymerase involving on the order of ~100 residues folds late in the mechanism and likely creates new protein−protein interfaces in doing so.

Numerous studies support the hypothesis that DNA melting occurs during the latter half of the mechanism (see, for example, *2*, *3*, *5*, *13*, *54*, *55*). DNA opening should expose amide-like functional groups on the bases (*38*), a process which should be favored by increasing urea concentration. Since the anticipated contribution of DNA opening to the urea dependence of $\ln(1/k_d)$ is in the opposite direction to what is observed, the amount of folding may be greater than predicted above.

What regions of Eσ^{70} could be disordered in the free enzyme, not fold in forming I_1 or in converting I_1 to the subsequent transition state, but then fold in the latter half of the mechanism of open complex formation? We tested whether either of two *E. coli* sequence insertions in the conserved polymerase architecture are responsible. Lack of density for residues in the downstream lobe of β (SI1: 226−350) and in the downstream β' clamp (SI3: 943−1130) in the EM structure of the *E. coli* core enzyme indicates that these regions are disordered, or folded, but flexibly tethered to ordered domains (*20*). Additionally, their points of insertion in the β jaw and β' downstream clamp (conserved regions G and G′; see Figure 9) make them likely candidates to participate in clamping DNA downstream of +10 (*20*, *44*, *56*−*58*). Consistent with their proposed role, deletion of either insertion destabilizes competitor-resistant complexes at λP_R relative to wild-type (Figure 2). However, the urea dependence of k_d is independent of either insertion within experimental uncertainty (Figure 2C), eliminating them as the origin of the effect. Indeed, SI3 has recently been shown to be folded, forming a β-sandwich-barrel hybrid domain that is connected to the trigger loop by two long, flexible tethers of ~13 amino acids each (*58*).

Prediction of Regions of Disorder in E. coli RNA Polymerase. The *E. coli* RNA polymerase has proved remarkably refractory to forming well-ordered crystals, suggesting that it is inherently more flexible than its thermophilic homologues and/or that the sequence insertions prevent highly ordered lattices from forming. To identify alternative candidates for regions that may be disordered in the *E. coli* enzyme, we applied the computer algorithm PONDR (see Experimental Procedures; *51*, *52*). PONDR has successfully predicted such regions from the primary amino acid sequence of other proteins (cf. *59*−*61*). From the set of sequences predicted to be disordered from the β and β' sequences of *T. aquaticus*, *T. thermophilus*, and *E. coli*, we considered sequences 15 amino acids in length or longer (the longer the region, the higher the probability that it is unfolded (*51*)). This set includes domains involved in creating subunit−subunit interfaces. Very possibly, these regions are unfolded before assembly and fold as part of interface formation during the assembly of core. Indeed, such folding coupled to assembly appears to be required for formation of the intertwined structure of core polymerase (*62*). Perhaps not surprisingly, the remaining predicted unfolded (dynamic or flexible) regions cluster around the perimeter of the polymerase jaws (shown in Figure 9 in crimson red). The most extensive regions of disorder occur in conserved regions G and G′ of the β' subunit. Notably, this region participates in interfaces formed in crystallization of the thermophilic polymerases; possibly, an ordered conformation of this flexible domain is selected, and ordering is coupled to crystallization. Crystallization of the *E. coli* enzyme may be disfavored relative to the thermophilic enzymes in part due to the insertion and flexibility of SI3 in this critical region (see above).

Proposal: Coupled Folding of β' Conserved Regions G and G′ Occurs in $I_2 \rightarrow RP_o$. Regions G and G′ of β' form the downstream mobile clamp; this clamp is proposed to bind promoter DNA downstream of the initiation bubble (*56*, *58*). Strikingly, deletion of conserved residues in this domain ($\beta'\Delta 1149-1190$) or a single amino acid substitution (β'G1161R) greatly destabilizes open complexes at the *lac*UV5, λP_R, RNA II, and *rrnB P1* promoters (*63*). Under the experimental conditions of that study, the half-time for dissociation of open complexes at *lac*UV5, RNA II, and λP_R decreased from several hours to several minutes, and a

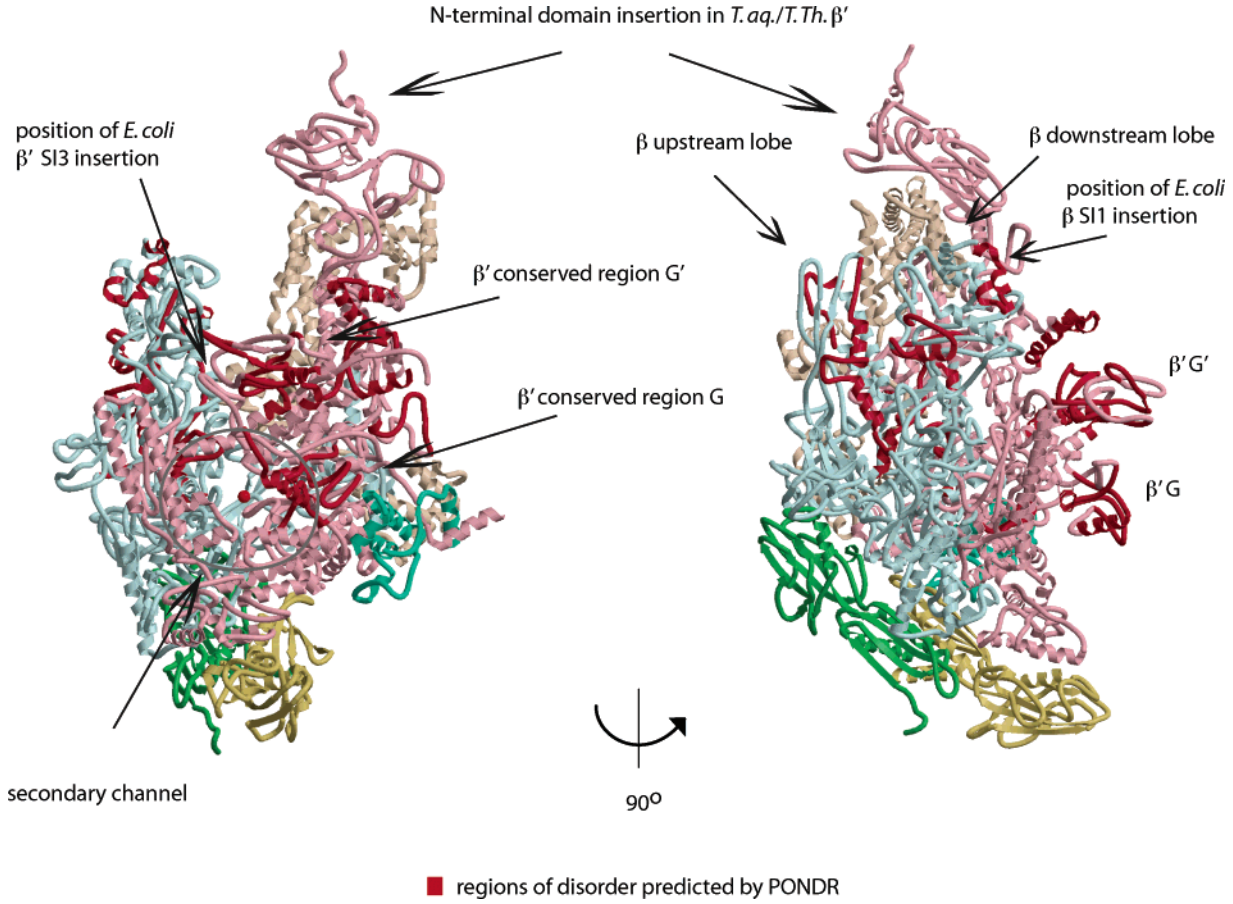

FIGURE 8: Regions of disorder in RNA polymerase holoenzyme predicted by PONDR (*50*, *51*). Cartoon based on PDB file 1IW7 (*14*). Regions (≥15 residues) predicted to lack a fixed tertiary structure in solution are highlighted in red. This data set excludes predicted disordered sequences that are found in subunit−subunit interfaces. PONDR regions cluster around the exterior of the jaws defined by β and β', and also include flexible regions in the active site channel (the "rudder" of β' (*T. thermophilus* residues 587−607, *E. coli* residues 311−331) and residues in two "fork" loops of β (*T. thermophilus* residues 399−417 and 441−454, *E. coli* residues 511−537 and 561−574). Regions predicted to have the most extensive degree of disorder are conserved regions G and G′ of β'. Subunit color scheme: α_I, green; α_{II} gold; β, light blue; β', pink; σ^A, bisque; ω, teal. Figure 8 was created using MolScript (*81*) and Raster3D (*82*).

comparable degree of destabilization was observed for the intrinsically unstable *rrnb P1* promoter−polymerase complex (*63*). The magnitude of this effect supports the hypothesis that this domain is not only critically involved in creating the open complex but that it also undergoes significant rearrangements to do so. The number of residues predicted from the urea dependence of k_d (∼120−140) is quantitatively consistent with the number of residues predicted by PONDR to be unfolded in the β' downstream clamp (∼120 residues). Thus, we propose that this region folds and binds late in open complex formation. On the basis of its position in the structure, it is likely that these rearrangements create new protein−protein interfaces between G and G′ and regions near the active site. The increase in $t_{1/2}$ of dissociation with increasing GB concentration is consistent with a net burial of anionic ASA in the formation of RP_o, possibly reflecting in part the folding and binding of the mobile clamp to the downstream DNA. A schematic representation of this and other proposed conformational changes (see below) deduced from these solute studies is shown in Figure 9.

Studies to date do not determine whether the proposed remodeling of regions G and G′ would occur in forming I_2 or in events that convert I_2 into RP_o. Possible clues are provided by recent advances in defining the mechanism of action of the small regulatory protein DksA. DksA critically modulates ribosomal promoter activity in response to changes to *in vivo* conditions, including amino acid starvation (*64*). Binding of DksA to RNA polymerase *in vitro* increases the dissociation rate of CR complexes at all promoters studied including λP_R (*65*), and effects of DksA and the alarmone ppGpp on dissociation are synergistic (*64*−*66*). On the basis of structural homology to GreA (*67*) and GreB (*68*), biochemical studies (*65*), and the EM structure of *E. coli* GreB and core polymerase (*57*), DksA has been proposed to bind in the secondary channel of polymerase (*65*). How does placement of DksA in the secondary channel destabilize open complexes?

In order for DksA to accelerate the decay of competitor-resistant complexes at λP_R, it must bind I_2 and/or the I_1-I_2 transition state more tightly than RP_o. No precedent exists for a protein to solely bind the transition state. For example, in the mechanism for catalysis by catalytic antibodies (generated using transition state analogues to achieve a high affinity for the transition state), the antibody is also observed to bind the substrate and product, albeit with reduced affinity relative to the transition state (*69*). Thus, it is likely that DksA binds to I_2. Why would positioning of DksA in the secondary channel disfavor RP_o formation relative to I_2?

As illustrated in Figure 8, the secondary channel (*62*) is defined entirely by β': two helices form one side of the

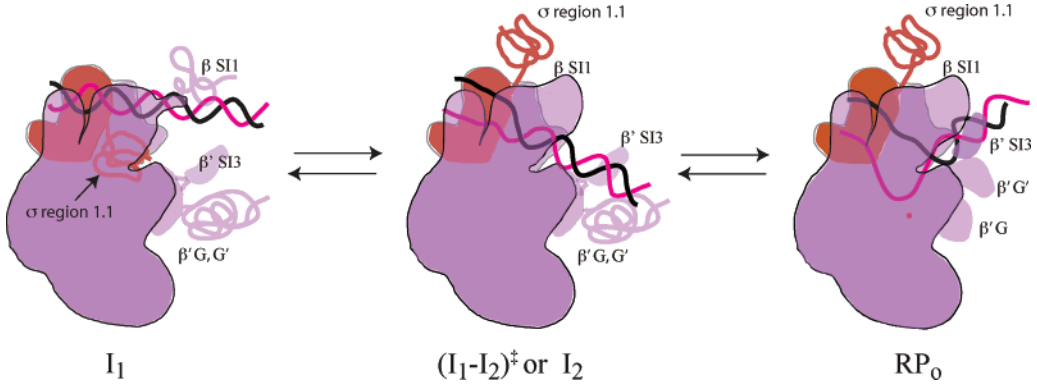

FIGURE 9: Schematic representation of the proposed conformational changes that convert I_1 to the transition state between and I_1 and I_2 (or I_2) and the subsequent changes that convert this species to RP_o at the λP_R promoter. Orientation of polymerase is the same as that shown in the right half of Figure 8 where the β subunit is closest to the viewer. The orientation here emphasizes events occurring in the active site channel and does not include DNA upstream of −12. Dimensions of holoenzyme and DNA are drawn approximately to scale; holoenzyme outline is based on PDB file 1IW7 (*14*), and the shape of *E. coli* β' SI3 is based on PDB file 2AUK (*58*). Coloring is core subunits (α, β, and β'; ω cannot be seen in this view), purple; σ, orange; nontemplate (nt) strand, black; template (t) strand, pink; and Mg^{2+} bound in the active site, red. In I_1, regions G and G′ of β' and SI1 of β are represented as being partially disordered. Downstream DNA is placed in the channel by a sharp bend at −11/−12 (*2*, *12*), but remains relatively base-paired downstream of this distortion. The negatively charged NTD domain of σ (region 1.1) is shown as lacking secondary structure and bound in the channel near the active site and the downstream lobe of β. Wrapping of upstream DNA in I_1 (not shown; (*12*)) positions β', G, G′, and SI3 in such a way to facilitate the release of 1.1. Isomerization of I_1 to I_2 is proposed to involve the ejection of 1.1 from the jaws, unmasking the active site. The release of 1.1 allows the DNA to descend further into the channel, permitting the downstream lobe of β to close and SI1 to fold. As the DNA descends, aromatic residues of σ capture bases in the −10 region of the nt strand, leading to DNA untwisting over ∼1 turn of the double helix. Repositioning and untwisting of the DNA in the channel triggers the conversion of $(I_1-I_2)^‡$ (or I_2) to RP_o; we hypothesize that basic residues in the channel bind DNA backbones of the nt and t strands to complete the formation of the transcription bubble in RP_o. DNA downstream of +5 is clamped by β', G, G′, and SI3. Position of SI3 in RP_o is based on ref *58*.

channel, (called the rim helices in ref *57*), the floor of the active site channel at the bottom, and by the F-helix on top. Importantly, the other side of the channel is created by β' region G. If this region is disordered, the secondary channel is not completely formed until it folds, and SI3 presumably occupies multiple positions. The proposed orientation of DksA in the secondary channel via its interface with the rim helices and Mg^{2+} in the active site (*65*) suggests to us that the C-terminal globular domain of DksA would sterically inhibit the rearrangement of the downstream clamp. In particular, the placement of SI3 in the position modeled by Chlenov et al. (*58*) may overlap the C-terminal domain of DksA. Thus, we hypothesize that the dynamic (unfolded) state of the downstream clamp preexists in free core and holoenzyme (DksA binds free core and holoenzyme *in vitro* (*64*, *65*)) and persists in I_1 and I_2, and that this conformational state (see Figure 9) favors DksA binding. While speculative, this line of reasoning leads to testable hypotheses: the downstream clamp of β' folds in the transition of I_2 to RP_o (see Figure 9) and DksA somehow blocks or disfavors this repositioning, thereby destabilizing RP_o relative to I_2.

Effects of Urea and GB on the Binding and Isomerization Steps in the Mechanism of RP_o Formation. Formation of the first kinetically significant intermediate at the λP_R promoter creates an interface involving ∼100 bp of promoter DNA: ·OH footprinting studies reveal that the DNA backbone is protected from at least −82 to +25 (Davis, C. A., manuscript in preparation). We proposed that DNase I protection to +25 in I_1 requires DNA binding in the β/β' jaws or pincers of polymerase (*2*, *11*), and we recently demonstrated that entry of DNA into the jaws is facilitated by the presence of DNA upstream of −47 (*12*). While footprinting reveals important information about DNA structure and interactions, information about possible conformational changes in RNAP in I_1 at λP_R was first inferred from the temperature and salt concentration dependence of k_a (*3*, *4*) and then from their effects on K_1 ((*2*), Kontur, W. S., manuscript in preparation). Here, the dependence of K_1 on urea and GB concentrations yields new insights into conformational changes occurring in I_1.

Unlike k_d, the dependence of K_1 on urea (Figure 7A, Table 2) provides no evidence for extensive protein folding or unfolding or DNA opening in forming I_1. In particular, the initial slope $(\partial \ln K_1/\partial m_{urea})_{m_4,m_5}$ at constant salt molality is small ($-0.3 \pm 0.3\ m^{-1}$); an approximate correction to constant activities of both KCl and $MgCl_2$ (see Experimental Procedures) yields a constant-salt-activity initial slope $(\partial \ln K_1/\partial m_{urea})_{a_4,a_5} = -0.7 \pm 0.3\ m^{-1}$. When eq 1 is used, this slope corresponds to burial of approximately 500 ± 200 Å^2 of polar amide surface in formation of I_1. What is region 1.1 of σ doing in this step? Can the negatively charged region 1.1 and downstream DNA co-occupy the jaws in I_1 or is 1.1 required to leave the active site channel in order for DNA to enter?

To address this critical question, we compared the experimentally predicted value of ΔASA_{amide} with an estimate based on available structural data and reasonable models for the downstream and upstream interfaces (Table 3). For wrapping of upstream DNA, we used the nucleosome and IHF as models. For downstream DNA interactions in the β/β' jaws (−5 to +20), we utilized our model of I_1 (*2*) which is based on DNaseI, ·OH, and $KMnO_4$ footprinting of I_1 at λP_R (*11*, *12*) and the high resolution *T. aquaticus* core structure (*70*). The relatively open jaw width (25−30 Å) in the core structure allows duplex DNA to enter "high" in the channel with little steric clash. The X-ray crystal structures of the −35 DNA−σ^A complex (*71*), and the αCTD−CAP−DNA cocrystal (*72*) allow a more accurate assessment of surface involved in contacts from −55 to ∼−26. In sum, modeling indicates that ∼440 Å^2 of polar amide surface is

Table 3: Estimates of Amounts of Polar Amide and Anionic Surface Buried in the First Kinetically Significant Intermedate (I_1) in Open Complex Formation at the λP_R Promoter

elements of the I_1 interface	DNA contacts (bp)	$-\Delta ASA_{amide}$ (Å^2)[a]	$-\Delta ASA_{anionic}$ (Å^2)[a]	model/comments
wrapping from ~−56 to −80	25	100	762	based on hydroxyl radical footprint (C.A.D., manuscript in preparation)
binding of two α CTD to ~−41 to −55	15	197	520	PDB file 1LB2 (*72*)
σ region 4/−35 DNA interactions	10	77	318	PDB file 1KU7 (*71*)
σ region 2/−10 DNA interactions	~5	ND	ND	
DNA bound in the "open" jaws from ~−5 to +20	25	70	200	based on the model of I_1 from ref *2*: DNA duplex "high" in jaws, jaw width about 25−30 Å in *T. aquaticus* core structure 1I6V (*70*)
total	~80	444	1800	missing an estimate for σ region 2/−10 DNA interactions, as well as any interactions with DNA between −35 and −10 regions
predicted based on $\partial \ln K_1/\partial m_{urea}$ at constant salt activity		500 ± 100		

[a] Estimates for amide and anionic surface (phosphate oxygens) buried in wrapping upstream DNA calculated using the average amount of $-\Delta ASA_{amide}$/bp (4.1 Å^2) and of $-\Delta ASA_{anionic}$/bp (30.5 Å^2) buried in the IHF−H′DNA (1IHF (*79*)) complex and in the nucleosome (1KX3 (*80*)). ND, not determined.

buried in contacts in I_1 (Table 3). Although we do not have a model for the σ region 2/−10 DNA complex, values in Table 3 suggest that the amount of amide ASA buried in this interface cannot exceed 100 Å^2.

Since the structural estimates presented in Table 3 explain most, if not all, of the effect of urea on K_1, the most straightforward hypothesis is that region 1.1 remains bound in the jaws in I_1. However, we cannot rule out the possibility that 1.1 exits but rebinds elsewhere, with no net amide exposure. If this region (residues 50−75 based on ·OH footprinting (*73*)) is entirely buried and then released into solution in an extended state (*17*), ~750 Å^2 of polar amide surface would be exposed, yielding a value of $\partial \ln K_1/\partial m_{urea}$ of ~+1 m^{-1}. Reconciliation of this prediction with the experimental observation requires burial of an additional ~750 Å^2 of polar amide ASA (eq 1). The absence of regions on polymerase likely to fold in this step, the relatively nonspecific interface formed in the β/β' jaws with DNA from −5 to +25, and the effect of GB on k_2 (below) suggest to us that 1.1 remains in the jaws in I_1.

The initial GB dependence of K_1 for formation of I_1 is modest; at constant KCl and $MgCl_2$ activity, the initial slope $(\partial \ln K_1/\partial m_{GB})_{a4,a5}$ is approximately 0.7 ± 0.4 m^{-1}. However, this value is only 40% of the GB dependence determined for the formation of the complex between LacI−SymL operator ($\partial \ln K_1/\partial m_{GB} = 1.8 \pm 0.2$ m^{-1} (*39*)). PDB file 1EFA (*40*) predicts ~630 Å^2 of anionic ASA are buried in the LacI dimer−SymL 20 bp oligomer complex, and Table 3 estimates ~1800 Å^2 of anionic ASA is buried in I_1. As in the case of LacI, qualitative, but not quantitative, agreement is found between the predicted slope of the GB dependence of K_1 for formation of I_1 and what is expected from structural models.

This disagreement might result in part from a compensating effect of weak GB−aromatic interactions, as discussed in the Introduction. Potential GB binding sites defined by multiple aromatic residues exist in region 2.3−2.4 of σ; interaction of these residues with GB might reduce their tendency to interact with the −10 region of the promoter in I_1. In addition, wrapping of upstream DNA in I_1 coupled to salt bridge disruption (*36*, *74*) may also complicate direct interpretation of GB effects on K_1. If the burial of phosphate oxygens is coupled to the rehydration of carboxylate surface, the opposing changes in anionic ASA are predicted to reduce the GB effect due to compensation. Because of the lack of appropriate models, calculation of $\Delta ASA_{anionic}$ in Table 3 requires an uncertain estimate for the burial of phosphate oxygen ASA.

Evidence for Release of Region 1.1 of σ^{70} in the Rate-Determining Isomerization Step. The dependences of the rate constant k_2 for the rate-determining conformational change in forward direction on solute concentrations and temperature provide thermodynamic clues about the process of converting I_1 to the subsequent $(I_1-I_2)^{\ddagger}$ transition state. In principle, these data can tell us whether this step is rate-determining because DNA opening is initiated, or because conformational changes in polymerase precede or nucleate opening. Unfortunately, but not surprisingly, the solute and temperature dependences suggest that multiple conformational changes occur in this step. The two unambiguous signatures of these conformational changes are the very large, facilitating effect of temperature on the rate constant (corresponding to a temperature-independent activation enthalpy of 34 ± 2 kcal mol^{-1} (*2*)) and the large retarding effect of GB concentration found in this study ($\partial \ln k_2/\partial m_{GB} = -0.6 \pm 0.1$ m^{-1}).

The sign of the GB effect on k_2 indicates that anionic biopolymer surface is exposed in this step. Since ·OH footprinting studies show that DNA phosphate surface is buried in interactions with polymerase during open complex formation, it is plausible to propose that GB detects the exposure of the highly negatively charged region of σ region 1.1 in the $(I_1-I_2)^{\ddagger}$ transition state. Release of 1.1 from its interactions with β and/or β' subunits in the jaws (*17*) is required to unmask the active site and allow interactions of start site DNA with these regions of polymerase. Movement of 1.1 may be the key step for initiating untwisting and opening of promoter DNA. Clearly, the step that exposes the active site is a logical target for regulation; in this proposal, unmasking would occur after promoter recognition is established and DNA downstream is placed in the jaws.

Intriguingly, this step exhibits no heat capacity change, no urea effect, and only a small destabilizing effect of salt concentration (Kontur, W. S., manuscript in preparation). No significant heat capacity change is expected if the overall

change in surface is predominantly (~70%) polar or charged (*2*, *75*). The absence of a urea effect means that no net exposure or burial of polar amide ASA occurs. The temperature, salt concentration, urea, and GB data taken together suggest to us that the exposure of 1.1 in the $(I_1-I_2)^{\ddagger}$ transition state is coupled to the folding of another region on polymerase. A logical candidate is SI1 of β. Positioned near the top of the downstream lobe of β (Figure 9), SI1 may be partially disordered in *E. coli* core: only ~50% of the expected volume is visible in the EM structure (*20*), and PONDR predicts that 47 of the ~125 residues in the N-terminus of SI1 are disordered. If binding of 1.1 in the jaws props the downstream jaw open (*15*) to allow DNA downstream of −5 to enter, release of 1.1 could lead to closure of the downstream lobe on DNA and thus to ordering of SI1 in $(I_1-I_2)^{\ddagger}$ (see schematic in Figure 9). Ordering of SI1 in the conversion of I_1 to $(I_1-I_2)^{\ddagger}$ would be consistent with the observation that deleting SI1 does not affect the urea dependence of later steps (k_d). The exchange of interactions with region 1.1 for contacts with downstream DNA in the jaws in this step is also consistent with the small salt concentration dependence of k_2. This mechanistic hypothesis predicts that urea will facilitate the isomerization step (k_2) with the mutant ΔSI1 polymerase at λP_R. Similarly, deletion of σ^{70} region 1.1 should eliminate the GB dependence of k_2 and introduce a urea dependence of k_2. These predictions are currently being investigated.

APPENDIX

Conversion of $(\partial \ln K_{obs}/\partial m_3)_{m_4,m_5}$ to $(\partial \ln K_{obs}/\partial m_3)_{a_4,a_5}$. The experimentally determined derivative is $(\partial \ln K_{obs}/\partial m_3)_{m_4,m_5}$ at constant temperature, pressure, and molalities of KCl and $MgCl_2$ (components 4 and 5, respectively). Here we relate this derivative to the derivative $(\partial \ln K_{obs}/\partial m_3)_{a_4,a_5}$ at constant salt activities and thereby eliminate the effect on $\ln K_{obs}$ of changes in salt activity brought about by changing urea or GB (component 3) concentration at constant salt molality. The basic mathematical relationship between $(\partial \ln K_{obs}/\partial m_3)_{m_4,m_5}$ and $(\partial \ln K_{obs}/\partial m_3)_{a_4,a_5}$ in an excess of solute components 3, 4, and 5 (relative to biopolymer participants) is

$$\left(\frac{\partial \ln K_{obs}}{\partial m_3}\right)_{a_4,a_5} = \left(\frac{\partial \ln K_{obs}}{\partial m_3}\right)_{m_4,m_5} + \left(\frac{\partial \ln K_{obs}}{\partial m_4}\right)_{m_3,m_5}\left(\frac{\partial m_4}{\partial m_3}\right)_{a_4,a_5} + \left(\frac{\partial \ln K_{obs}}{\partial m_5}\right)_{m_3,m_4}\left(\frac{\partial m_5}{\partial m_3}\right)_{a_4,a_5} \quad \text{(A1)}$$

The additive correction terms in eq A1 are evaluated using experimental data. For component 4 (KCl),

$$\left(\frac{\partial \ln K_{obs}}{\partial m_4}\right)_{m_3=0} \cong SK^{o(3)}_{obs\,4}/m_4 \quad \text{(A2)}$$

where

$$SK^{o(3)}_{obs\,4} \equiv \left(\frac{\partial \ln K_{obs}}{\partial \ln[4]}\right)_{m_3=0,m_5} \cong \left(\frac{\partial \ln K_{obs}}{\partial \ln m_4}\right)_{m_3=0,m_5}$$

On the basis of Euler reciprocity,

$$\left(\frac{\partial m_4}{\partial m_3}\right)_{a_4,a_5} = -\frac{\partial \mu_4/\partial m_3}{\partial \mu_4/\partial m_4} = -\frac{\partial \mu_3/\partial m_4}{\partial \mu_4/\partial m_4} \quad \text{(A3)}$$

where

$$\partial \mu_3/\partial m_4 = RT\Delta Osm_{34}/m_3 m_4 \quad \text{(A4)}$$

and

$$\partial \mu_4/\partial m_4 = 2RT(1+\epsilon_{\pm})_{m_3,m_5=0}/m_4 \quad \text{(A5)}$$

where $\epsilon_{\pm} = \partial \ln \gamma_{\pm}/\partial m_4$ (where $\gamma_{\pm}$ is the mean ionic activity coefficient of the salt).

An analogous derivation (parallel to eqs A2−A5) holds for component 5 ($MgCl_2$) involving $SK^{o(3)}_{obs\,5} \equiv (\partial \ln K_{obs}/\partial(\ln[5]))_{m_3=0,m_4}$ except that $\partial \mu_5/\partial m_5 = 3RT(1+\epsilon_{\pm})_{m_3,m_4=0}/m_5$.

Combining equations A2−A5 with eq 1 yields

$$\left(\frac{\partial \ln K_{obs}}{\partial m_3}\right)_{a_4,a_5} \cong \left(\frac{\partial \ln K_{obs}}{\partial m_3}\right)_{m_4,m_5} + \left(\frac{SK^{o(3)}_{obs\,4}\Delta Osm_{34}}{2m_3 m_4(1+\epsilon_{\pm})_{m_3 m_5=0}}\right) + \left(\frac{SK^{o(3)}_{obs\,5}\Delta Osm_{35}}{3m_3 m_5(1+\epsilon_{\pm})_{m_3 m_4=0}}\right) \quad \text{(A6)}$$

The correction is shown here for an equilibrium constant K_{obs}, but is applicable to either equilibrium or rate constants. Equation A6 is only applicable to the relevant experimental situation where urea, GB, KCl, and $MgCl_2$ are in excess of the biopolymers and to the analysis of the initial dependence of $\ln K_{obs}$ on solute concentration (m_3).

Analysis of data from a previous study on the KCl concentration dependence of the kinetics (in 10 mM $MgCl_2$ at 37 °C) (*1*) yields Sk_{a4} ($= SK_1 + Sk_2$) ≅ −4.0 ± 0.7 and $Sk_{d\,4}$ ≅ 3.2 ± 0.7 over the ranges 100−180 mM KCl and 120−200 mM KCl, respectively. A later study showed that the log−log dependence of k_a on $MgCl_2$ concentration in the absence of a 1−1 salt is approximately one-half that observed on KCl concentration in the absence of $MgCl_2$ ($Sk_{a\,5} \cong (1/2)Sk_{a\,4}$) and that k_d is much less dependent on $MgCl_2$ concentration than it is on KCl concentration (*76*); thus, we assume $Sk_{a\,5} = -2.0 \pm 0.4$ and $Sk_{d\,5} = 0.4 \pm 0.1$ here. Recent experimental data shows that the dependence of k_2 on salt concentration is much smaller than the dependence of K_1 (Kontur, W. S., manuscript in preparation); here, no significant errors are introduced by assuming that $Sk_2 \cong 0$ and $Sk_a \cong SK_1$.

In eqs A4 and A6, $\Delta Osm_{34}/m_3 m_4 = Osm(m_3,m_4) - Osm(m_3) - Osm(m_4)$, where $Osm(m_3)$ and $Osm(m_4)$ are osmolalities of two component solutions at the same molality as that of these solutes in the three component solution with osmolality $Osm(m_3,m_4)$. (The analogous definition applies to ΔOsm_{35}.) Values of $\Delta Osm_{34}/m_3 m_4$ (0.09 ± 0.02 for urea−KCl and 0.12 ± 0.01 for GB−KCl (*37*)) and $\Delta Osm_{35}/m_3 m_5$ (0.32 ± 0.09 for urea−$MgCl_2$ and 0.6 ± 0.1 for GB−$MgCl_2$) were obtained by vapor pressure osmometry (Capp, M. W., unpublished work). For KCl solutions in the range 0.2−0.43 *m*, $(1+\epsilon_{\pm})_{m_3,m_5=0} = 0.893 \pm 0.001$ (*77*); for $MgCl_2$ in the range 0.053−0.546 *m*, $(1+\epsilon_{\pm})_{m_3,m_4=0} = 0.99 \pm 0.02$ (calculated from published data (*78*)).

ACKNOWLEDGMENT

We thank Laurel Pegram (UW-Madison) for assistance with preliminary dissociation experiments as a function of urea. We are extremely grateful to Irina Artsimovitch (Ohio State University) and Vladimir Svetlov (Ohio State University) for generous gifts of plasmids, protein purification expertise, stimulating discussions, and sharing manuscripts in advance of publication and to Seth Darst (The Rockefeller University) for discussion, sharing models, coordinates of SI3, and ref *58* in advance of publication. We appreciate the many valuable discussions with Craig Bingman, Robert Landick, and Record lab colleagues over the course of this work.

SUPPORTING INFORMATION AVAILABLE

Association kinetic data describing CR complex formation between Eσ^{70} RNAP and λP_R promoter DNA as a function of urea (0, 0.21, 0.42, and 0.63 *m*) at 17.1 °C in BB_{urea}^{dissoc}. This material is available free of charge via the Internet at http://pubs.acs.org.

REFERENCES

1. Roe, J. H., Burgess, R. R., and Record, M. T., Jr. (1984) Kinetics and mechanism of the interaction of *Escherichia coli* RNA polymerase with the λP_R promoter, *J. Mol. Biol. 176*, 495−522.
2. Saecker, R. M., Tsodikov, O. V., McQuade, K. L., Schlax, P. E., Jr., Capp, M. W., and Record, M. T., Jr. (2002) Kinetic studies and structural models of the association of *E. coli* σ^{70} RNA polymerase with the λP_R promoter: large scale conformational changes in forming the kinetically significant intermediates, *J. Mol. Biol. 319*, 649−671.
3. Roe, J. H., Burgess, R. R., and Record, M. T., Jr. (1985) Temperature dependence of the rate constants of the *Escherichia coli* RNA polymerase-λP_R promoter interaction. Assignment of the kinetic steps corresponding to protein conformational change and DNA opening, *J. Mol. Biol. 184*, 441−453.
4. Roe, J. H., and Record, M. T., Jr. (1985) Regulation of the kinetics of the interaction of *Escherichia coli* RNA polymerase with the λP_R promoter by salt concentration, *Biochemistry 24*, 4721−4726.
5. Buc, H., and McClure, W. R. (1985) Kinetics of open complex formation between *Escherichia coli* RNA polymerase and the lac UV5 promoter. Evidence for a sequential mechanism involving three steps, *Biochemistry 24*, 2712−2723.
6. Kadesch, T. R., Rosenberg, S., and Chamberlin, M. J. (1982) Binding of *Escherichia coli* RNA polymerase holoenzyme to bacteriophage T7 DNA. Measurements of binding at bacteriophage T7 promoter A1 using a template competition assay, *J. Mol. Biol. 155*, 1−29.
7. Rosenberg, S., Kadesch, T. R., and Chamberlin, M. J. (1982) Binding of *Escherichia coli* RNA polymerase holoenzyme to bacteriophage T7 DNA. Measurements of the rate of open complex formation at T7 promoter A, *J. Mol. Biol. 155*, 31−51.
8. Johnson, R. S., and Chester, R. E. (1998) Stopped-flow kinetic analysis of the interaction of *Escherichia coli* RNA polymerase with the bacteriophage T7 A1 promoter, *J. Mol. Biol. 283*, 353−370.
9. Sclavi, B., Zaychikov, E., Rogozina, A., Walther, F., Buckle, M., and Heumann, H. (2005) Real-time characterization of intermediates in the pathway to open complex formation by *Escherichia coli* RNA polymerase at the T7A1 promoter, *Proc. Natl. Acad. Sci. U.S.A. 102*, 4706−4711.
10. Li, X. Y., and McClure, W. R. (1998) Characterization of the closed complex intermediate formed during transcription initiation by *Escherichia coli* RNA polymerase, *J. Biol. Chem. 273*, 23549−23557.
11. Craig, M. L., Tsodikov, O. V., McQuade, K. L., Schlax, P. E., Jr., Capp, M. W., Saecker, R. M., and Record, M. T., Jr. (1998) DNA footprints of the two kinetically significant intermediates in formation of an RNA polymerase−promoter open complex: evidence that interactions with start site and downstream DNA induce sequential conformational changes in polymerase and DNA, *J. Mol. Biol. 283*, 741−756.
12. Davis, C. A., Capp, M. W., Record, M. T., Jr., and Saecker, R. M. (2005) The effects of upstream DNA on open complex formation by *Escherichia coli* RNA polymerase, *Proc. Natl. Acad. Sci. U.S.A. 102*, 285−290.
13. Schickor, P., Metzger, W., Werel, W., Lederer, H., and Heumann, H. (1990) Topography of intermediates in transcription initiation of *E. coli*, *EMBO J. 9*, 2215−2220.
14. Vassylyev, D. G., Sekine, S., Laptenko, O., Lee, J., Vassylyeva, M. N., Borukhov, S., and Yokoyama, S. (2002) Crystal structure of a bacterial RNA polymerase holoenzyme at 2.6 Å resolution, *Nature 417*, 712−719.
15. Murakami, K. S., Masuda, S., and Darst, S. A. (2002) Structural basis of transcription initiation: RNA polymerase holoenzyme at 4 Å resolution, *Science 296*, 1280−1284.
16. Murakami, K. S., and Darst, S. A. (2003) Bacterial RNA polymerases: the wholo story. *Curr. Opin. Struct. Biol. 13*, 31−39.
17. Mekler, V., Kortkhonjia, E., Mukhopadhyay, J., Knight, J., Revyakin, A., Kapanidis, A. N., Niu, W., Ebright, Y. W., Levy, R., and Ebright, R. H. (2002) Structural organization of bacterial RNA polymerase holoenzyme and the RNA polymerase−promoter open complex. *Cell 108*, 599−614.
18. Murakami, K. S., Masuda, S., Campbell, E. A., Muzzin, O., and Darst, S. A. (2002) Structural basis of transcription initiation: an RNA polymerase holoenzyme−DNA complex, *Science 296*, 1285−1290.
19. Callaci, S., Heyduk, E., and Heyduk, T. (1999) Core RNA polymerase from *E. coli* induces a major change in the domain arrangement of the sigma 70 subunit, *Mol. Cell 3*, 229−238.
20. Darst, S. A., Opalka, N., Chacon, P., Polyakov, A., Richter, C., Zhang, G., and Wriggers, W. (2002) Conformational flexibility of bacterial RNA polymerase, *Proc. Natl. Acad. Sci. U.S.A. 99*, 4296−4301.
21. Spassky, A., Kirkegaard, K., and Buc, H. (1985) Changes in the DNA structure of the lacUV5 promoter during formation of an open complex with *Escherichia coli* RNA polymerase, *Biochemistry 24*, 2723−2731.
22. Buckle, M., Pemberton, I. K., Jacquet, M. A., and Buc, H. (1999) The kinetics of sigma subunit directed promoter recognition by *E. coli* RNA polymerase, *J. Mol. Biol. 285*, 955−964.
23. McKane, M., and Gussin, G. N. (2000) Changes in the 17 bp spacer in the P_R promoter of bacteriophage lambda affect steps in open complex formation that precede DNA strand separation, *J. Mol. Biol. 299*, 337−349.
24. Bartlett, M. S., Gaal, T., Ross, W., and Gourse, R. L. (1998) RNA polymerase mutants that destabilize RNA polymerase-promoter complexes alter NTP-sensing by rrn P1 promoters, *J. Mol. Biol. 279*, 331−345.
25. Cowing, D. W., Mecsas, J., Record, M. T., Jr., and Gross, C. A. (1989) Intermediates in the formation of the open complex by RNA polymerase holoenzyme containing the sigma factor σ^{32} at the groE promoter, *J. Mol. Biol. 210*, 521−530.
26. McKane, M., Malone, C., and Gussin, G. N. (2001) Mutations at position −10 in the λP_R promoter primarily affect conversion of the initial closed complex (RP_c) to a stable, closed intermediate (RP_i), *Biochemistry 40*, 2023−2031.
27. Schroeder, L. A., and deHaseth, P. L. (2005) Mechanistic differences in promoter DNA melting by *Thermus aquaticus* and *Escherichia coli* RNA polymerases, *J. Biol. Chem. 280*, 17422−17429.
28. McQuade, K. L. (1996) Ph.D. Thesis, University of Wisconsin−Madison, Madison, WI.
29. Spolar, R. S., and Record, M. T., Jr. (1994) Coupling of local folding to site-specific binding of proteins to DNA, *Science 263*, 777−784.
30. Spolar, R. S., Livingstone, J. R., and Record, M. T., Jr. (1992) Use of liquid hydrocarbon and amide transfer data to estimate contributions to thermodynamic functions of protein folding from the removal of nonpolar and polar surface from water, *Biochemistry 31*, 3947−3955.
31. Murphy, K. P., and Freire, E. (1992) Thermodynamics of structural stability and cooperative folding behavior in proteins, *Adv. Protein Chem. 43*, 313−361.
32. Myers, J. K., Pace, C. N., and Scholtz, J. M. (1995) Denaturant m-values and heat capacity changes: relation to changes in accessible surface areas of protein unfolding, *Protein Sci. 4*, 2138−2148.

33. Ferrari, M. E., and Lohman, T. M. (1994) Apparent heat capacity change accompanying a nonspecific protein−DNA interaction. *Escherichia coli* SSB tetramer binding to oligodeoxyadenylates, *Biochemistry 33*, 12896−12910.
34. Kozlov, A. G., and Lohman, T. M. (1999) Adenine base unstacking dominates the observed enthalpy and heat capacity changes for the *Escherichia coli* SSB tetramer binding to single-stranded oligoadenylates, *Biochemistry*, *38*, 7388−7397.
35. Kozlov, A. G., and Lohman, T. M. (2000) Large contributions of coupled protonation equilibria to the observed enthalpy and heat capacity changes for ssDNA binding to *Escherichia coli* SSB protein, *Proteins* (Suppl. 4), 8−22.
36. Holbrook, J. A., Tsodikov, O. V., Saecker, R. M., and Record, M. T., Jr. (2001) Specific and non-specific interactions of integration host factor with DNA: thermodynamic evidence for disruption of multiple IHF surface salt-bridges coupled to DNA binding, *J. Mol. Biol. 310*, 379−401.
37. Scholtz, J. M., Barrick, D., York, E. J., Stewart, J. M., and Baldwin, R. L. (1995) Urea unfolding of peptide helices as a model for interpreting protein unfolding, *Proc. Natl. Acad. Sci. U.S.A. 92*, 185−189.
38. Hong, J., Capp, M. W., Anderson, C. F., Saecker, R. M., Felitsky, D. J., Anderson, M. W., and Record, M. T., Jr. (2004) Preferential interactions of glycine betaine and of urea with DNA: implications for DNA hydration and for effects of these solutes on DNA stability. *Biochemistry 43*, 14744−58.
39. Hong, J., Capp, M. W., Saecker, R. M., and Record, M. T., Jr. (2005) Use of urea and glycine betaine to quantify coupled folding and probe the burial of DNA phosphates in lac repressor−lac operator binding, *Biochemistry 44*, 16896−16911.
40. Bell, C. E., and Lewis, M. (2000) A closer view of the conformation of the lac repressor bound to operator, *Nat. Struct. Biol. 7*, 209−214.
41. Spronk, C. A., Slijper, M., van Boom, J. H., Kaptein, R., and Boelens, R. (1996) Formation of the hinge helix in the lac repressor is induced upon binding to the lac operator, *Nat. Struct. Biol. 3*, 916−919.
42. Schiefner, A., Breed, J., Bosser, L., Kneip, S., Gade, J., Holtmann, G., Diederichs, K., Welte, W., and Bremer, E. (2004) Cation−pi interactions as determinants for binding of the compatible solutes glycine betaine and proline betaine by the periplasmic ligand-binding protein ProX from *Escherichia coli*, *J. Biol. Chem. 279*, 5588−5596.
43. Felitsky, D. J., Cannon, J. G., Capp, M. W., Hong, J., Van Wynsberghe, A. W., Anderson, C. F., and Record, M. T., Jr. (2004) The exclusion of glycine betaine from anionic biopolymer surface: why glycine betaine is an effective osmoprotectant but also a compatible solute, *Biochemistry 43*, 14732−14743.
44. Artsimovitch, I., Svetlov, V., Murakami, K. S., and Landick, R. (2003) Co-overexpression of *Escherichia coli* RNA polymerase subunits allows isolation and analysis of mutant enzymes lacking lineage-specific sequence insertions, *J. Biol. Chem. 278*, 12344−12355.
45. Studier, F. W. (2005) Protein production by auto-induction in high-density shaking cultures, *Protein Expression Purif. 41*, 207−234.
46. Borukhov, S., and Goldfarb, A. (1993) Recombinant *Escherichia coli* RNA polymerase: purification of individually overexpressed subunits and in vitro assembly, *Protein Expression Purif. 4*, 503−511.
47. Craig, M. L., Suh, W. C., and Record, M. T., Jr. (1995) HO· and DNase I probing of Eσ^{70} RNA polymerase−λP_R promoter open complexes: Mg^{2+} binding and its structural consequences at the transcription start site, *Biochemistry 34*, 15624−15632.
48. Saecker, R. M., Tsodikov, O. V., Capp, M. W., and Record, M. T., Jr. (2003) Rapid quench mixing to quantify kinetics of steps in association of *Escherichia coli* RNA polymerase with promoter DNA, *Methods Enzymol. 370*, 535−546.
49. Tsodikov, O. V., and Record, M. T., Jr. (1999) General method of analysis of kinetic equations for multistep reversible mechanisms in the single-exponential regime: application to kinetics of open complex formation between Eσ^{70} RNA polymerase and λP_R promoter DNA, *Biophys. J. 76*, 1320−1329.
50. Hong, J., Capp, M. W., Anderson, C. F., and Record, M. T. (2003) Preferential interactions in aqueous solutions of urea and KCl, *Biophys. Chem. 105*, 517−532.
51. Romero, P., Obradovic, Z., Li, X., Garner, E. C., Brown, C. J., and Dunker, A. K. (2001) Sequence complexity of disordered protein, *Proteins 42*, 38−48.
52. Li, X., Romero, P., Rani, M., Dunker, A. K., and Obradovic, Z. (1999) Predicting protein disorder for N-, C-, and internal regions, *Genome Inf. Ser. 10*, 30−40.
53. Kamali-Moghaddam, M., and Geiduschek, E. P. (2003) Thermoirreversible and thermoreversible promoter opening by two *Escherichia coli* RNA polymerase holoenzymes, *J. Biol. Chem. 278*, 29701−29709.
54. Walter, G., Zillig, W., Palm, P., and Fuchs, E. (1967) Initiation of DNA-dependent RNA synthesis and the effect of heparin on RNA polymerase, *Eur. J. Biochem. 3*, 194−201.
55. Helmann, J. D., and deHaseth, P. L. (1999) Protein−nucleic acid interactions during open complex formation investigated by systematic alteration of the protein and DNA binding partners, *Biochemistry 38*, 5959−5967.
56. Korzheva, N., Mustaev, A., Kozlov, M., Malhotra, A., Nikiforov, V., Goldfarb, A., and Darst, S. A. (2000) A structural model of transcription elongation, *Science 289*, 619−625.
57. Opalka, N., Chlenov, M., Chacon, P., Rice, W. J., Wriggers, W., and Darst, S. A. (2003) Structure and function of the transcription elongation factor GreB bound to bacterial RNA polymerase, *Cell 114*, 335−345.
58. Chlenov, M., Masuda, S., Murakami, K. S., Nikiforov, V., Darst, S. A., and Mustaev, A. (2005) Structure and function of lineage-specific sequence insertions in the bacterial RNA polymerase β' subunit, *J. Mol. Biol. 353*, 138−154.
59. Karlin, D., Ferron, F., Canard, B., and Longhi, S. (2003) Structural disorder and modular organization in *Paramyxovirinae* N and P, *J. Gen. Virol. 84*, 3239−3252.
60. Tozawa, K., Macdonald, C. J., Penfold, C. N., James, R., Kleanthous, C., Clayden, N. J., and Moore, G. R. (2005) Clusters in an intrinsically disordered protein create a protein-binding site: the TolB-binding region of colicin E, *Biochemistry 44*, 11496−11507.
61. Dyson, H. J., and Wright, P. E. (2005) Intrinsically unstructured proteins and their functions, *Nat. Rev. Mol. Cell Biol. 6*, 197−208.
62. Zhang, G., Campbell, E. A., Minakhin, L., Richter, C., Severinov, K., and Darst, S. A. (1999) Crystal structure of *Thermus aquaticus* core RNA polymerase at 3.3 Å resolution, *Cell 98*, 811−824.
63. Ederth, J., Artsimovitch, I., Isaksson, L. A., and Landick, R. (2002) The downstream DNA jaw of bacterial RNA polymerase facilitates both transcriptional initiation and pausing, *J. Biol. Chem. 277*, 37456−37463.
64. Paul, B. J., Barker, M. M., Ross, W., Schneider, D. A., Webb, C., Foster, J. W., and Gourse, R. L. (2004) DksA: a critical component of the transcription initiation machinery that potentiates the regulation of rRNA promoters by ppGpp and the initiating NTP, *Cell 118*, 311−322.
65. Perederina, A., Svetlov, V., Vassylyeva, M. N., Tahirov, T. H., Yokoyama, S., Artsimovitch, I., and Vassylyev, D. G. (2004) Regulation through the secondary channel−structural framework for ppGpp−DksA synergism during transcription, *Cell 118*, 297−309.
66. Paul, B. J., Berkmen, M. B., and Gourse, R. L. (2005) DksA potentiates direct activation of amino acid promoters by ppGpp, *Proc. Natl. Acad. Sci. U.S.A. 102*, 7823−7828.
67. Stebbins, C. E., Borukhov, S., Orlova, M., Polyakov, A., Goldfarb, A., and Darst, S. A. (1995) Crystal structure of the GreA transcript cleavage factor from *Escherichia coli*, *Nature 373*, 636−640.
68. Koulich, D., Orlova, M., Malhotra, A., Sali, A., Darst, S. A., and Borukhov, S. (1997) Domain organization of *Escherichia coli* transcript cleavage factors GreA and GreB, *J. Biol. Chem. 272*, 7201−7210.
69. Lerner, R. A., Benkovic, S. J., and Schultz, P. G. (1991) At the crossroads of chemistry and immunology: catalytic antibodies, *Science 252*, 659−667.
70. Campbell, E. A., Korzheva, N., Mustaev, A., Murakami, K., Nair, S., Goldfarb, A., and Darst, S. A. (2001) Structural mechanism for rifampicin inhibition of bacterial RNA polymerase, *Cell 104*, 901−912.
71. Campbell, E. A., Muzzin, O., Chlenov, M., Sun, J. L., Olson, C. A., Weinman, O., Trester-Zedlitz, M. L., and Darst, S. A. (2002) Structure of the bacterial RNA polymerase promoter specificity sigma subunit, *Mol. Cell 9*, 527−539.
72. Benoff, B., Yang, H., Lawson, C. L., Parkinson, G., Liu, J., Blatter, E., Ebright, Y. W., Berman, H. M., and Ebright, R. H. (2002)

Structural basis of transcription activation: the CAP-alpha CTD−DNA complex, *Science 297*, 1562−1566.
73. Nagai, H., and Shimamoto, N. (1997) Regions of the *Escherichia coli* primary sigma factor σ^{70} that are involved in interaction with RNA polymerase core enzyme, *Genes Cells 2*, 725−734.
74. Saecker, R. M., and Record, M. T., Jr. (2002) Protein surface salt bridges and paths for DNA wrapping, *Curr. Opin. Struct. Biol. 12*, 311−319.
75. Holbrook, J. A., Capp, M. W., Saecker, R. M., and Record, M. T., Jr. (1999) Enthalpy and heat capacity changes for formation of an oligomeric DNA duplex: interpretation in terms of coupled processes of formation and association of single-stranded helices, *Biochemistry 38*, 8409−8422.
76. Suh, W. C., Leirmo, S., and Record, M. T., Jr. (1992) Roles of Mg^{2+} in the mechanism of formation and dissociation of open complexes between *Escherichia coli* RNA polymerase and the λP_R promoter: kinetic evidence for a second open complex requiring Mg^{2+}, *Biochemistry 31*, 7815−7825.
77. Archer, D. G. (1999) Thermodynamic properties of the KCl−H_2O system, *J. Phys. Chem. Ref. Data 28*, 1−17.
78. Weast, R. C. *Handbook of Chemistry and Physics*; CRC Press, Cleveland, OH, 1975; p D-235.
79. Rice, P. A., Yang, S., Mizuuchi, K., and Nash, H. A. (1996) Crystal structure of an IHF−DNA complex: a protein-induced DNA U-turn, *Cell 87*, 1295−306.
80. Davey, C. A., Sargent, D. F., Luger, K., Maeder, A. W., and Richmond, T. J. (2002) Solvent mediated interactions in the structure of the nucleosome core particle at 1.9 Å resolution, *J. Mol. Biol. 319*, 1097−1113.
81. Kraulis, P. J. (1991) MOLSCRIPT: a program to produce both detailed and schematic plots of protein structures, *J. Appl. Crystallogr. 24*, 946−950.
82. Merritt, E. A., and Bacon, D. J. (1997) Raster3D: photorealistic molecular graphics, *Methods Enzymol. 277*, 505−524.

BI051835V